

# Divide-and-Conquer with Sequential Monte Carlo

F. Lindsten<sup>1,3</sup>, A. M. Johansen<sup>2</sup>, C. A. Naesseth<sup>3</sup>, B. Kirkpatrick<sup>4</sup>,  
T. B. Schön<sup>5</sup>, J. A. D. Aston<sup>1</sup>, and A. Bouchard-Côté<sup>6</sup>

30 June 2015

## Abstract

We propose a novel class of Sequential Monte Carlo (SMC) algorithms, appropriate for inference in probabilistic graphical models. This class of algorithms adopts a divide-and-conquer approach based upon an auxiliary tree-structured decomposition of the model of interest, turning the overall inferential task into a collection of recursively solved sub-problems. The proposed method is applicable to a broad class of probabilistic graphical models, *including* models with loops. Unlike a standard SMC sampler, the proposed Divide-and-Conquer SMC employs multiple independent populations of weighted particles, which are resampled, merged, and propagated as the method progresses. We illustrate empirically that this approach can outperform standard methods in terms of the accuracy of the posterior expectation and marginal likelihood approximations. Divide-and-Conquer SMC also opens up novel parallel implementation options and the possibility of concentrating the computational effort on the most challenging sub-problems. We demonstrate its performance on a Markov random field and on a hierarchical logistic regression problem.

**Keywords:** Bayesian methods, Graphical models, Hierarchical models, Particle filters

## 1 Introduction

Sequential Monte Carlo (SMC) methods are a popular class of algorithms for approximating some sequence of probability distributions of interest,  $(\pi_t(\mathbf{x}_t) : t = 1, \dots, n)$ . This is done by simulating, for each distribution in the sequence, a collection of  $N$  particles  $\{\mathbf{x}_t^i\}_{i=1}^N$  with corresponding nonnegative importance weights  $\{\mathbf{w}_t^i\}_{i=1}^N$ , such that the weighted empirical distribution  $\hat{\pi}_t^N(d\mathbf{x}_t) := (\sum_j \mathbf{w}_t^j)^{-1} \sum_i \mathbf{w}_t^i \delta_{\mathbf{x}_t^i}(d\mathbf{x}_t)$  approximates  $\pi_t$ . The weighted particles are generated sequentially, in the sense that the particles generated at iteration  $t$  depends on the particles generated up to iteration  $t - 1$ .

The most well-known application of SMC is to the filtering problem in general state-space hidden Markov models, see e.g., Doucet and Johansen (2011) and references therein. However, these methods are much more generally applicable and there has been much recent

---

\*1 University of Cambridge, 2 University of Warwick, 3 Linköping University, 4 University of Miami, 5 Uppsala University, 6 University of British Columbia. Address for Correspondence: Fredrik Lindsten, Signal Processing Laboratory, CUED, Trumpington Street, Cambridge, CB2 3PU. Email: [fredrik.lindsten@eng.cam.ac.uk](mailto:fredrik.lindsten@eng.cam.ac.uk).

interest in using SMC for sampling from probability distributions that do not arise from chain-shaped probabilistic graphical models (PGMs). This typically involves using SMC to target a sequence of auxiliary distributions which are constructed to admit the original distribution as an appropriate marginal (Del Moral et al., 2006). Examples include likelihood tempering (Del Moral et al., 2006), data tempering (Chopin, 2002), and sequential model decompositions (Bouchard-Côté et al., 2012; Naesseth et al., 2014), to mention a few.

For many statistical models of interest, however, a *sequential* decomposition might not be the most natural, nor computationally efficient, way of approaching the inference problem. In this contribution we propose an extension of the classical SMC framework, Divide-and-Conquer SMC (D&C-SMC), which we believe will further widen the scope of SMC samplers and provide efficient computational tools for Bayesian inference within a broad class of probabilistic models.

The idea underlying D&C-SMC is that an approximation can be made to any multivariate distribution by splitting the collection of model variables into *disjoint* sets and defining, for each of these sets, a suitable auxiliary target distribution. Sampling from these distributions is typically easier than sampling from the original distribution and can be done in parallel, whereafter the results are merged to provide a solution to the original problem of interest (correcting for the discrepancy between the approximating and exact distributions by importance sampling techniques). Using the divide-and-conquer methodology, we recurse and repeat this procedure for each of the components. This corresponds to breaking the overall inferential task into a collection of simpler problems. At any intermediate iteration of the D&C-SMC algorithm we maintain multiple independent sets of weighted particles, which are subsequently merged and propagated as the algorithm progresses, using rules similar to those employed in standard SMC. The proposed method inherits some of the theoretical guarantees of standard SMC methods. In particular, our simulation scheme can be used to provide *exact approximations* of costly or intractable MCMC algorithms, via the particle MCMC methodology (Andrieu et al., 2010).

Furthermore, we introduce a method for constructing the aforementioned decompositions for a broad class of PGMs of interest, which we call *self-similar graphical models*. To construct auxiliary distributions, we remove edges and nodes in a PGM of interest, creating smaller connected components as sub-graphical models. These sub-graphical models are then recursively decomposed as well. Note that this decomposition does not assume that the PGM of interest is tree-shaped. Indeed, we demonstrate that the proposed methodology is effective not only when the model has an obvious hierarchical structure (for example, Figure 3), but also in cases where the hierarchical decomposition is artificial (Figure 5). In either case, one iteratively exploits solutions to easier sub-problems as a first step in the solution of a more complex problem.

We conclude this section with a summary of the structure of the remainder of the paper. Section 2 provides details on the background of the work presented here: algorithms upon which it builds and those to which it is related. The basic D&C-SMC and decomposition methodology is presented in Section 3, including a discussion of its theoretical properties. A number of methodological extensions are presented in Section 4 and two realistic applications are presented in Section 5. The paper concludes with a discussion.

## 2 Background and problem formulation

### 2.1 Problem formulation

We let  $\pi$  denote a probability distribution of interest, termed the *target distribution*. With a slight abuse of notation, we also denote its density by  $\pi(\mathbf{x})$ ,  $\mathbf{x} \in \mathbf{X}$  (with respect to an anonymous reference measure). The set  $\mathbf{X}$  is called the *state space*, and could be discrete, continuous or mixed (we assume throughout the paper that all spaces are Polish and equipped with Borel  $\sigma$ -algebras). We assume that the density  $\pi$  can be written as  $\pi(\mathbf{x}) = \gamma(\mathbf{x})/Z$ , where the unnormalized density  $\gamma(\mathbf{x})$  can be computed point-wise, whereas evaluating the *normalization constant*  $Z = \int \gamma(\mathbf{x})d\mathbf{x}$  may be computationally challenging. The two problems with we are concerned are (1) approximating the normalization constant  $Z$ , and (2), computing integrals under  $\pi$  of some *test function*  $f : \mathbf{X} \rightarrow \mathbb{R}$ ,  $\int f(\mathbf{x})\pi(\mathbf{x})d\mathbf{x}$ , where  $f(\mathbf{x})$  can be computed point-wise. In a Bayesian context, (1) corresponds to approximating the marginal likelihood of the observed data, and (2), computing the posterior expectation of some function,  $f$ , of the parameters and latent variables,  $\mathbf{x}$ .

### 2.2 Probabilistic graphical models

Problems (1) and (2) often arise in the context of PGMs, a formalism to encode dependencies between random variables in a probabilistic model. Two sorts of graphical structures are commonly used by statisticians to describe model dependencies: the Bayesian Network (Pearl, 1985), which summarizes the conditional independence structure of a Bayesian model using a directed acyclic graph, and undirected graphs, which are often used to describe models specified via the full conditional distribution of each node such as Markov random fields (see below) and many spatial models such as conditional autoregressions (Besag, 1974). Here, we focus on the abstract factor graph formalism, and remind the reader that the two formalisms mentioned above can be easily converted to factor graphs; see, e.g., Bishop (2006) for details.

Two assumptions are required in order to write a model as a factor graph. First, that the state space,  $\mathbf{X}$ , takes the form of a product space,  $\mathbf{X} = \mathbf{X}_n = \tilde{\mathbf{X}}_1 \times \tilde{\mathbf{X}}_2 \times \dots \times \tilde{\mathbf{X}}_n$ . It is convenient to define the set of *variables*,  $V$ , corresponding to the elements of this factorization,  $1, 2, \dots, n$ . Second, that the unnormalized density  $\gamma$  can be decomposed as,  $\gamma(\mathbf{x}_n = (\tilde{\mathbf{x}}_1, \dots, \tilde{\mathbf{x}}_n)) = \prod_{\phi \in F} \phi(S_\phi(\tilde{\mathbf{x}}_1, \dots, \tilde{\mathbf{x}}_n))$ , where  $F$  is a set of *factors* and the function  $S_\phi$  returns a sub-vector of  $(\tilde{\mathbf{x}}_1, \dots, \tilde{\mathbf{x}}_n)$  containing those elements upon which factor  $\phi$  depends.

Under these assumptions, a factor graph can be defined as a bipartite graph, where the set of vertices is given by  $F \cup V$ , and where we place an edge between a variable  $v \in V$  and a factor  $\phi \in F$  whenever the function  $\phi$  depends on  $\tilde{\mathbf{X}}_v$ , i.e. when  $\mathbf{x}_v$  is included in the vector returned by  $S_\phi(\mathbf{x}_1, \dots, \mathbf{x}_n)$ . Throughout the paper, we use the convention that a variable with a tilde denotes a variable taking values in a single dimension ( $\tilde{\mathbf{x}}_n \in \tilde{\mathbf{X}}_n$ ), while variables without tilde are elements of a product space ( $\mathbf{x}_n = (\tilde{\mathbf{x}}_1, \dots, \tilde{\mathbf{x}}_n) \in \mathbf{X}_n = \tilde{\mathbf{X}}_1 \times \dots \tilde{\mathbf{X}}_n$ ).

## 2.3 Sequential Monte Carlo

Sequential Monte Carlo (SMC) methods are a class of sampling algorithms able to address problems (1) and (2) defined in Section 2.1. More precisely, SMC can be used to simulate from a sequence of probability distributions defined on a sequence of spaces of increasing dimension. Let  $\pi_t(\mathbf{x}_t)$ , with  $\mathbf{x}_t := (\tilde{\mathbf{x}}_1, \dots, \tilde{\mathbf{x}}_t)$ , be a PDF defined on the product space

$$\mathbf{X}_t = \tilde{\mathbf{X}}_1 \times \tilde{\mathbf{X}}_2 \times \dots \times \tilde{\mathbf{X}}_t. \quad (1)$$

Furthermore, as above, assume that  $\pi_t(\mathbf{x}_t) = \gamma_t(\mathbf{x}_t)/Z_t$  where  $\gamma_t$  can be evaluated point-wise, but where the normalizing constant  $Z_t$  is computationally intractable. SMC provides a way to sequentially approximate the sequence of distributions  $\pi_1, \pi_2, \dots, \pi_n$ . As a byproduct, it also provides *unbiased* estimates of the normalizing constants  $Z_1, Z_2, \dots, Z_n$  (Del Moral, 2004, Prop. 7.4.1).

The SMC approximation of  $\pi_t$  at iteration  $t$  ( $1 \leq t \leq n$ ) takes the form of a *particle population*. This population consists in a collection of  $N$  pairs of *particles* and *weights*:  $\{\mathbf{x}_t^i, \mathbf{w}_t^i\}_{i=1}^N$ , where  $\mathbf{x}_t^i \in \mathbf{X}_t$  and  $\mathbf{w}_t^i \geq 0$ . The particle population provides an approximation of  $\pi_t$ , in the (weak) sense that expectations of a (sufficiently regular) *test* function,  $f$ , with respect to the discrete probability distribution obtained after normalizing the weights,

$$\hat{\pi}_t^N(\cdot) := \frac{1}{\sum_{j=1}^N \mathbf{w}_t^j} \sum_{i=1}^N \mathbf{w}_t^i \delta_{\mathbf{x}_t^i}(\cdot), \quad (2)$$

approximate the expectation of that test function under  $\pi_t$ :

$$\int \pi_t(\mathbf{x}_t) f(\mathbf{x}_t) d\mathbf{x}_t \approx \left( \sum_{j=1}^N \mathbf{w}_t^j \right)^{-1} \sum_{i=1}^N \mathbf{w}_t^i f(\mathbf{x}_t^i).$$

One can consider test functions of direct interest (as well as considering the weak convergence of the approximating distributions which can be established under various conditions) for example, one would use  $f(\mathbf{x}) = \mathbf{x}$  to approximate a mean, and  $f(\mathbf{x}) = \mathbf{1}_A(\mathbf{x})$  to approximate the probability that  $\mathbf{x} \in A$ .

We review here the simplest type of SMC algorithm, Sequential Importance Resampling (SIR), and refer the reader to Doucet and Johansen (2011) for a more in-depth exposition. Pseudo-code for the SIR method is given in Algorithm 1. We present the algorithm in a slightly non-standard recursive form because it will be convenient to present the proposed D&C-SMC algorithm recursively, and presenting SIR in this way makes it easier to compare the two algorithms. Furthermore, since the focus of this paper is “static” problems (i.e., we are not interested in online inference, such as filtering), the sequential nature of the procedure need not be emphasized. For ease of notation, we allow the procedure to be called for  $t = 0$ , which returns an “empty” set of particles and, by convention,  $\gamma_0(\emptyset) = 1$ . (Hence, we do not need to treat the cases  $t = 1$  and  $t > 1$  separately in the algorithm.) The main steps of the algorithm, *resampling*, *proposal sampling*, and *weighting*, are detailed below.

Resampling (Line 3), in its simplest form, consists of sampling  $N$  times from the previous population approximation  $\hat{\pi}_{t-1}^N$ , as defined in (2). This is equivalent to sampling the number of copies to be made of each particle from a multinomial distribution with number of trials  $N$

---

**Algorithm 1**  $\text{sir}(t)$ 


---

1. If  $t = 0$ , return  $(\{\emptyset, 1\}_{i=1}^N, 1)$ .
  2.  $(\{\mathbf{x}_{t-1}^i, \mathbf{w}_{t-1}^i\}_{i=1}^N, \widehat{Z}_{t-1}^N) \leftarrow \text{sir}(t-1)$ .
  3. Resample  $\{\mathbf{x}_{t-1}^i, \mathbf{w}_{t-1}^i\}_{i=1}^N$  to obtain the unweighted particle population  $\{\tilde{\mathbf{x}}_{t-1}^i, 1\}_{i=1}^N$ .
  4. For particle  $i = 1, \dots, N$ :
    - (a) Simulate  $\tilde{\mathbf{x}}_t^i \sim q_t(\cdot | \tilde{\mathbf{x}}_{t-1}^i)$ .
    - (b) Set  $\mathbf{x}_t^i = (\tilde{\mathbf{x}}_{t-1}^i, \tilde{\mathbf{x}}_t^i)$ .
    - (c) Compute  $\mathbf{w}_t^i = \frac{\gamma_t(\mathbf{x}_t^i)}{\gamma_{t-1}(\tilde{\mathbf{x}}_{t-1}^i) q_t(\tilde{\mathbf{x}}_t^i | \tilde{\mathbf{x}}_{t-1}^i)}$ .
  5. Compute  $\widehat{Z}_t^N = \left\{ \frac{1}{N} \sum_{i=1}^N \mathbf{w}_t^i \right\} \widehat{Z}_{t-1}^N$ .
  6. Return  $(\{\mathbf{x}_t^i, \mathbf{w}_t^i\}_{i=1}^N, \widehat{Z}_t^N)$ .
- 

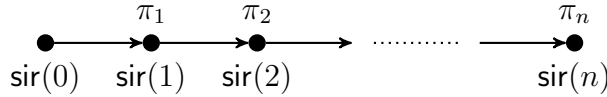


Figure 1: Computational flow of SIR (analogous for any SMC sampler). Each node corresponds to a call to `sir`, the labels above show the corresponding target distribution, and the arrows illustrate the recursive dependencies of the algorithm. Note that this “computational graph” of SMC is a chain, even if the sequence of target distributions does not correspond to a chain-structured PGM.

and probability vector  $(\mathbf{w}_{t-1}^1, \dots, \mathbf{w}_{t-1}^N) / (\sum_{i=1}^N \mathbf{w}_{t-1}^i)$ . Since resampling is done with replacement, a given particle can be resampled zero, one, or multiple times. Informally, the goal of the resampling step is to prune particles of low weights in order to focus computation on the promising parts of the state space. This is done in a way that preserves the asymptotic guarantees of importance sampling. After resampling, the weights are reset to  $1/N$ , since the weighting is instead encoded in the random multiplicities of the particles. Note that more sophisticated resampling methods are available, see, e.g., Douc et al. (2005). Proposal sampling (Line 4), is based on user-provided proposal densities  $q_t(\tilde{\mathbf{x}}_t | \mathbf{x}_{t-1})$ . For each particle  $\tilde{\mathbf{x}}_{t-1}^i \in \mathbf{X}_{t-1}$  output from the resampling stage, we sample a successor state  $\tilde{\mathbf{x}}_t^i \sim q_t(\cdot | \tilde{\mathbf{x}}_{t-1}^i)$ . The sampled successor is a single state  $\tilde{\mathbf{x}}_t^i \in \tilde{\mathbf{X}}_t$  which is appended to  $\tilde{\mathbf{x}}_{t-1}^i$ , to form a sample for the  $t$ -th product space,  $\mathbf{x}_t^i = (\tilde{\mathbf{x}}_{t-1}^i, \tilde{\mathbf{x}}_t^i) \in \mathbf{X}_t$ . Finally, weighting (Line 4c) is used to correct for the discrepancy between  $\pi_{t-1}(\tilde{\mathbf{x}}_{t-1}^i) q_t(\tilde{\mathbf{x}}_t^i | \tilde{\mathbf{x}}_{t-1}^i)$  and the new target  $\pi_t(\tilde{\mathbf{x}}_{t-1}^i, \tilde{\mathbf{x}}_t^i)$ . Importantly, weighting can be performed on the unnormalized target densities  $\gamma_t$  and  $\gamma_{t-1}$ . The algorithm returns a particle-based approximation  $\widehat{\pi}_t^N$  of  $\pi_t$ , as in (2), as well as an unbiased estimate  $\widehat{Z}_t^N$  of  $Z_t$  (Line 5). In practice, an important improvement to this basic algorithm is to perform resampling only when particle degeneracy is severe. This can be done by monitoring the effective sample size (ESS):  $(\sum_{i=1}^N \mathbf{w}_t^i)^2 / \sum_{i=1}^N (\mathbf{w}_t^i)^2$ , and by resampling only when ESS is smaller than some threshold, say  $N/2$  (Kong et al., 1994). In Figure 1 we illustrate the execution flow of the algorithm as arising from the recursive function calls.

The sequence of *target distributions*  $\{\pi_t : t = 1, \dots, n\}$  can be constructed in many

different ways, which largely explains the generality and success of SMC. The most basic construction, which is the classical application of SMC, arises from chain-structured factor graphs (for example, state-space models or hidden Markov models). For a chain-graph, the joint PDF can be factorized as  $\pi(\mathbf{x}) = \frac{1}{Z} \prod_{t=1}^n \phi_t(\tilde{\mathbf{x}}_{t-1}, \tilde{\mathbf{x}}_t)$ , where  $\mathbf{x} = (\tilde{\mathbf{x}}_1, \dots, \tilde{\mathbf{x}}_n)$ ; see Section 2.2. (As above, to simplify the notation we have, without loss of generality, introduced a “dummy variable”  $\tilde{\mathbf{x}}_0 = \emptyset$ .) To simulate from the target distribution, the standard SIR algorithm employs a sequence of *intermediate distributions*:  $\pi_t(\mathbf{x}_t) \propto \prod_{s=1}^t \phi_s(\tilde{\mathbf{x}}_{s-1}, \tilde{\mathbf{x}}_s)$ , where  $\mathbf{x}_t = (\tilde{\mathbf{x}}_1, \dots, \tilde{\mathbf{x}}_t)$ ,  $\tilde{\mathbf{x}}_s \in \tilde{\mathcal{X}}_s$ . Each  $\pi_t$  can be written as  $\gamma_t/Z_t$ , where again  $\gamma_t$  can be evaluated point-wise, but  $Z_t$  is hard to compute. Importantly, we also have that  $\pi_n = \pi$  by construction. In fact, it is possible to make use of similar *sequential decompositions* even when the original graph is not a chain (Naesseth et al., 2014), as long as it is possible to find a sequence of auxiliary distributions defined on increasing subsets of the model variables.

## 2.4 SMC samplers and tempering

Another common approach is to make use of a sequence of auxiliary distributions for which we are interested only in one of the marginals. Suppose that the densities of interest are defined over spaces which are not product spaces,  $\tilde{\pi}_t : \tilde{\mathcal{X}}_t \rightarrow [0, \infty)$ . For example, we may have  $\tilde{\pi}_t(\tilde{\mathbf{x}}) \propto (\tilde{\pi}(\tilde{\mathbf{x}}))^{\alpha_t}$  as a tempered target distribution, with  $\tilde{\mathcal{X}}_t = \tilde{\mathcal{X}}_{t-1} = \dots = \tilde{\mathcal{X}}_1$ , and  $q_t(\tilde{\mathbf{x}}_t | \tilde{\mathbf{x}}_{t-1})$  derived from a local MCMC move. We can transform problems of this type into a form suitable for SMC by using an auxiliary construction proposed by Del Moral et al. (2006), which can be viewed as a (substantial) generalization of the annealed importance sampling method (Neal, 2001).

The construction used by Del Moral et al. (2006) is to re-introduce a sequence of distributions defined on product spaces  $\mathcal{X}_t = \tilde{\mathcal{X}}_1 \times \dots \times \tilde{\mathcal{X}}_t$  by defining,

$$\pi_t(\mathbf{x}_t) = \tilde{\pi}_t(\tilde{\mathbf{x}}_t) \prod_{s=1}^{t-1} L_s(\tilde{\mathbf{x}}_s | \tilde{\mathbf{x}}_{s+1}), \quad (3)$$

where  $\mathbf{x}_t = (\tilde{\mathbf{x}}_1, \dots, \tilde{\mathbf{x}}_t) \in \mathcal{X}_t$  as before. In the above,  $L_s$  is a transition kernel from  $\tilde{\mathcal{X}}_{s+1}$  to  $\tilde{\mathcal{X}}_s$ —for instance an MCMC kernel—chosen by the user. For any choice of these *backward kernels*,  $\pi_t$  admits  $\tilde{\pi}_t$  as a marginal by construction, and it can thus be used as a proxy for the original target distribution  $\tilde{\pi}_t$ . Standard SMC algorithms can then be applied to the sequence of auxiliary distributions  $\pi_t$ ,  $t = 1, \dots, n$ . Using the structure of  $\pi_t$  in (3), the weight computation (Line 4c of Algorithm 1) is given by:

$$\mathbf{w}_t^i = \frac{\tilde{\gamma}_t(\tilde{\mathbf{x}}_t^i)}{\tilde{\gamma}_{t-1}(\tilde{\mathbf{x}}_{t-1}^i)} \frac{L_{t-1}(\tilde{\mathbf{x}}_{t-1}^i | \tilde{\mathbf{x}}_t^i)}{q_t(\tilde{\mathbf{x}}_t^i | \tilde{\mathbf{x}}_{t-1}^i)}, \quad (4)$$

where  $\tilde{\gamma}_t \propto \tilde{\pi}_t$ . While the backward kernels  $L_t$  are formally arbitrary (subject to certain support restrictions), they will critically influence the estimator variance. If  $q_t$  is a  $\tilde{\pi}_{t-1}$ -reversible MCMC kernel, a typical choice is  $L_{t-1} = q_t$  which results in a cancellation in the weight expression (4):  $\mathbf{w}_t^i = \tilde{\gamma}_t(\tilde{\mathbf{x}}_t^i)/\tilde{\gamma}_{t-1}(\tilde{\mathbf{x}}_{t-1}^i)$ . See Del Moral et al. (2006) for further details and guidance on the selection of the backward kernels.

## 2.5 Related work

Before presenting the new methodology in Section 3 we note that a number of related ideas have appeared in the literature, although all have differed in key respects from the approach described in the next section.

Koller et al. (1999) and Briers et al. (2005); Sudderth et al. (2010) address belief propagation using importance sampling and SMC, respectively, and these methods feature coalescence of particle systems, although they do not provide samples targeting a distribution of interest in an *exact* sense (Andrieu et al., 2010). In contrast, the method proposed here yields consistent estimates of the marginals and normalization constant, even when approximating a graphical model with loops. Moreover, our method can handle variables with constrained or discrete components, while much of the existing literature relies on Gaussian approximations which may not be practical in these cases.

Coalescence of particle systems in a different sense is employed by Jasra et al. (2008) who also use multiple populations of particles; here the state space of the full parameter vector is partitioned, rather than the parameter vector itself. The *island particle model* of Vergé et al. (2014) employs an ensemble of particle systems which themselves interact according to the usual rules of SMC, with every particle system targeting the same distribution over the full set of variables. The *local particle filtering* approach by Rebeschini and van Handel (2013) attempts to address degeneracy (in a hidden Markov model context) via an (inexact) localisation technique. Numerous authors have proposed custom SMC algorithms for the purpose of inferring the structure of a latent tree, see Teh et al. (2008); Bouchard-Côté et al. (2012); Lakshminarayanan et al. (2013). These methods generally employ a single particle population. In contrast, our method assumes a known tree decomposition, and uses several particle populations.

## 3 Methodology

The proposed methodology is useful when the inference problem described in Section 2.1 can be decomposed into a “tree of auxiliary distributions”, as defined in Section 3.1 below. We present the basic D&C-SMC method in Section 3.2, followed by fundamental convergence results in Section 3.3. Thereafter, we provide a concrete strategy for constructing the aforementioned tree-structured auxiliary distributions on which the D&C-SMC algorithm operates. This strategy applies to many directed and undirected graphical modelling scenarios of practical interest (including models with cycles). It should be noted that, as with standard SMC algorithms, a range of techniques are available to improve on the basic method presented in this section, and we discuss several possible extensions in Section 4.

### 3.1 Tree structured auxiliary distributions

The proposed D&C-SMC methodology generalizes the classical SMC framework from sequences (or chains) to trees. As noted in Section 2, the SMC methodology is a general framework for simulating from essentially any *sequence* of distributions. Any such sequence can be organized on a chain, with subsequent distributions being associated with neighbouring nodes on the chain; see Figure 1. Note that the graph notion here is used to describe

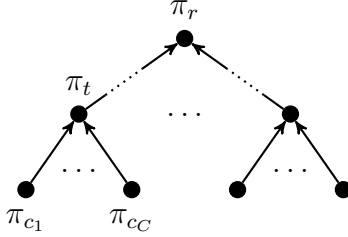


Figure 2: Computational flow of D&C-SMC. Each node corresponds to a target distribution  $\{\pi_t : t \in T\}$  and, thus, to a call to D&C-SMC (Algorithm 2). The arrows illustrate the computational flow of the algorithm via its recursive dependencies.

the execution flow of the algorithm, and the sequence of distributions organized on the chain does not necessarily correspond to a chain-structured PGM.

In a similar way, D&C-SMC operates on a *tree of distributions*, which need not correspond to a tree-structured PGM. Specifically, as in Section 2.3, assume that we have a collection of (auxiliary) distributions,  $\{\pi_t : t \in T\}$ . However, instead of taking the index set  $T$  to be nodes in a sequence,  $T = \{1, 2, \dots, n\}$ , we generalize  $T$  to be nodes in a tree. For all  $t \in T$ , let  $\mathcal{C}(t) \subset T$  denote the children of node  $t$ , with  $\mathcal{C}(t) = \emptyset$  if  $t$  is a leaf, and let  $r \in T$  denote the root of the tree. We assume  $\pi_t$  to have a density, also denoted by  $\pi_t$ , defined on a set  $\mathbf{X}_t$ . We call such a collection a tree structured auxiliary distributions a *tree decomposition* of the target distribution  $\pi$  (introduced in Section 2.1) if it has two properties. First, the root distribution is required to coincide with the target distribution,  $\pi_r = \pi$ . The second is a consistency condition: we require that the spaces on which the node distributions are defined are constructed recursively as

$$\mathbf{X}_t = \left( \otimes_{c \in \mathcal{C}(t)} \mathbf{X}_c \right) \times \tilde{\mathbf{X}}_t \quad (5)$$

where the “incremental” set  $\tilde{\mathbf{X}}_t$  can be chosen arbitrarily (in particular,  $\tilde{\mathbf{X}}_t = \emptyset$  for all  $t$  in some proper subset of the nodes in  $T$  is a valid choice). Note that the second condition mirrors the product space condition (1). That is, the distributions  $\{\pi_t : t \in T\}$  are defined on spaces of increasing dimensions as we move towards the root from the leaves of the tree.

Figure 2 illustrates the execution flow of the D&C-SMC algorithm (which is detailed in the subsequent section), which performs inference for the distributions  $\{\pi_t : t \in T\}$  from leaves to root in the tree. As pointed out above, the computational tree  $T$  does not necessarily correspond to a tree-structured PGM. Nevertheless, when the PGM of interest *is* in fact a tree, the computational flow of the algorithm can be easily related to the structure of the model (just as the computational flow of standard SMC is easily understood when the PGM is a chain, although the SMC framework is in fact more general). Let us therefore consider an example of how the target distributions  $\{\pi_t : t \in T\}$  can be constructed in such a case, to provide some intuition for the proposed inference strategy before getting into the details of the algorithm.

*Example* (Hierarchical models). Consider the simple tree-structured Bayesian network of Figure 3 (rightmost panel), with three observations  $y_{1:3}$ , and five latent variables  $\tilde{\mathbf{x}}_{1:5}$ . The distribution of interest is the posterior  $p(\tilde{\mathbf{x}}_{1:5} | y_{1:3})$ . To put this in the notation introduced above, we define  $\mathbf{x}_5 = \tilde{\mathbf{x}}_{1:5}$  and  $\pi(\mathbf{x}_5) = \pi_5(\mathbf{x}_5) = p(\tilde{\mathbf{x}}_{1:5} | y_{1:3})$ . To obtain a tree decomposition



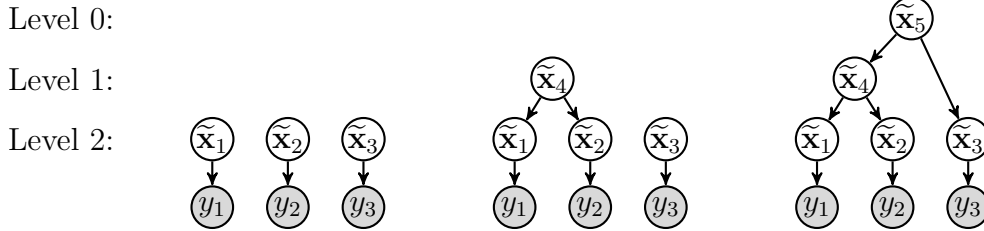


Figure 3: Decomposition of a hierarchical Bayesian model.

of  $\pi_5$  we can make use of the hierarchical structure of the PGM. By removing the root node  $\tilde{\mathbf{x}}_5$  we obtain two decoupled components (Figure 3, middle) for which we can define the auxiliary target distributions  $\pi_4(\mathbf{x}_4) = p(\mathbf{x}_4 | y_{1:2})$  and  $\pi_3(\mathbf{x}_3) = p(\xi_3 | y_3)$ , respectively, where  $\mathbf{x}_4 = (\tilde{\mathbf{x}}_1, \tilde{\mathbf{x}}_2, \tilde{\mathbf{x}}_4)$  and  $\mathbf{x}_3 = \tilde{\mathbf{x}}_3$ . If the marginal priors for the root nodes in the decomposed models (here,  $p(\tilde{\mathbf{x}}_4)$  and  $p(\tilde{\mathbf{x}}_3)$ ) are intractable to compute, we can instead define the auxiliary distribution  $\pi_t(\mathbf{x}_t)$ ,  $t = 3, 4$ , using an arbitrary “artificial prior”  $u_t(\tilde{\mathbf{x}}_t)$  for its root (similar to the two-filter smoothing approach of Briers et al. (2010)). This arbitrariness is ultimately corrected for by importance weighting and does not impinge upon the validity of the proposed inference algorithm (see Section 3.3), although the choice of  $u_t$  can of course affect the computational efficiency of the algorithm. Finally, by repeating this procedure, we can further decompose  $\pi_4(\mathbf{x}_4)$  into two components,  $\pi_1(\mathbf{x}_1)$  and  $\pi_2(\mathbf{x}_2)$ , as illustrated in Figure 3 (left). The target distributions  $\{\pi_t(\mathbf{x}_t) : t \in \{1, \dots, 5\}\}$  can be organised on a tree (with the same graph topology as the PGM under study, excluding the observed variables) which satisfies the conditions for being a tree decomposition of the sought posterior  $p(\tilde{\mathbf{x}}_{1:5} | y_{1:3})$ .

In Section 3.4 we formalise the decomposition strategy illustrated in the example above, and also generalise it to a broader class of, so called, self-similar PGMs.

### 3.2 Divide-and-Conquer Sequential Importance Resampling

We now turn to the description of the D&C-SMC algorithm—a Monte Carlo procedure for approximating the target distribution  $\pi = \pi_r$  based on the auxiliary distributions  $\{\pi_t : t \in T\}$ . For pedagogical purposes, we start by presenting the simplest possible implementation of the algorithm, which can be thought of as the analogue to the SIR implementation of SMC. Several possible extensions are discussed in Section 4.

As in standard SMC, D&C-SMC approximates each  $\pi_t$  by a collection of weighted samples, also referred to as a particle population. Unlike a standard SMC sampler, however, the method maintains multiple *independent* populations of weighted particles,  $(\{\mathbf{x}_t^i, \mathbf{w}_t^i\}_{i=1}^N : t \in T_k)$ , which are propagated and merged as the algorithm progresses. Here  $T_k \subset T$  is the set of indices of “active” target distributions at iteration  $k$ ,  $1 \leq k \leq \text{depth}(T)$ .

The D&C-SMC algorithm uses a bottom-up approach to simulate from the auxiliary target distributions defined on the tree, by repeated resampling, proposal, and weighting steps, which closely mirror standard SMC. We describe the algorithm by specifying the operations that are carried out at each node of the tree, leading to a recursive definition of the method. For  $t \in T$ , we define a procedure `dc_smc(t)` which returns, (1) a weighed particle population  $\{\mathbf{x}_t^i, \mathbf{w}_t^i\}_{i=1}^N$  approximating  $\pi_t$  as  $\hat{\pi}_t^N$  in Equation (2), and (2) an estimator  $\hat{Z}_t^N$

---

**Algorithm 2**  $\text{dc\_smc}(t)$ 


---

1. For  $c \in \mathcal{C}(t)$ :
    - (a)  $(\{\mathbf{x}_c^i, \mathbf{w}_c^i\}_{i=1}^N, \widehat{Z}_c^N) \leftarrow \text{dc\_smc}(c)$ .
    - (b) Resample  $\{\mathbf{x}_c^i, \mathbf{w}_c^i\}_{i=1}^N$  to obtain the equally weighted particle system  $\{\check{\mathbf{x}}_c^i, 1\}_{i=1}^N$ .
  2. For particle  $i = 1, \dots, N$ :
    - (a) If  $\check{\mathbf{X}}_t \neq \emptyset$ , simulate  $\tilde{\mathbf{x}}_t^i \sim q_t(\cdot | \check{\mathbf{x}}_{c_1}^i, \dots, \check{\mathbf{x}}_{c_C}^i)$ , where  $(c_1, c_2, \dots, c_C) = \mathcal{C}(t)$ ; else  $\tilde{\mathbf{x}}_t^i \leftarrow \emptyset$ .
    - (b) Set  $\mathbf{x}_t^i = (\check{\mathbf{x}}_{c_1}^i, \dots, \check{\mathbf{x}}_{c_C}^i, \tilde{\mathbf{x}}_t^i)$ .
    - (c) Compute  $\mathbf{w}_t^i = \frac{\gamma_t(\mathbf{x}_t^i)}{\prod_{c \in \mathcal{C}(t)} \gamma_c(\check{\mathbf{x}}_c^i) q_t(\tilde{\mathbf{x}}_t^i | \check{\mathbf{x}}_{c_1}^i, \dots, \check{\mathbf{x}}_{c_C}^i)}$ .
  3. Compute  $\widehat{Z}_t^N = \left\{ \frac{1}{N} \sum_{i=1}^N \mathbf{w}_t^i \right\} \prod_{c \in \mathcal{C}(t)} \widehat{Z}_c^N$ .
  4. Return  $(\{\mathbf{x}_t^i, \mathbf{w}_t^i\}_{i=1}^N, \widehat{Z}_t^N)$ .
- 

of the normalizing constant  $Z_t$  (such that  $\pi_t(\mathbf{x}_t) = \gamma_t(\mathbf{x}_t)/Z_t$ ). The procedure is given in Algorithm 2.

The first step of the algorithm is to acquire, for each child node  $c \in \mathcal{C}(t)$ , a particle approximation of  $\pi_c$  by a recursive call (Line 1a). Jointly, these particle populations provide an approximation of the product measure,

$$\otimes_{c \in \mathcal{C}(t)} \pi_c(d\mathbf{x}_c) \approx \otimes_{c \in \mathcal{C}(t)} \widehat{\pi}_c^N(d\mathbf{x}_c). \quad (6)$$

Note that this point-mass approximation has support on  $N^C$ ,  $C = |\mathcal{C}(t)|$ , points, although these support points are implicitly given by the  $NC$  unique particles (assuming no duplicates among the particles in the individual child populations).

To obtain a computationally manageable approximation of the product measure, we generate  $N$  samples from the approximation in (6). This is equivalent to performing standard multinomial resampling for each child particle population (Line 1b), obtaining equally weighted samples  $\{\check{\mathbf{x}}_c^i, 1\}_{i=1}^N$  for each  $c$ , and for all  $i = 1, \dots, N$ , combining all indices  $i$  of the  $c$  lists to create  $N$  equally weighted tuples,  $(\check{\mathbf{x}}_{c_1}^i, \dots, \check{\mathbf{x}}_{c_C}^i, 1)_{i=1}^N$ . This basic merging strategy can thus be implemented in  $O(N)$  computational cost, since there is no need to explicitly form the approximation of the product measure in (6).

The latter, resampling-based, description of how the child populations are merged provide natural extensions to the methodology, e.g. by using low-variance resampling schemes (e.g., Carpenter et al. (1999)) and adaptive methods that monitor effective sample size to perform resampling only when particle degeneracy is severe (Kong et al., 1994).

*Remark 1.* Note, however, that if we perform resampling amongst the child populations separately and then combine the resulting particles in this way, we require  $\mathbb{P}(\check{\mathbf{x}}_c^i = \mathbf{x}_c^j) = (\sum_{l=1}^N \mathbf{w}_c^l)^{-1} \mathbf{w}_c^j$ ,  $j = 1, \dots, N$ , for each  $i = 1, \dots, N$ , since the particles are combined based on their indices (i.e., it is not enough that the marginal equality  $\sum_{i=1}^N \mathbb{P}(\check{\mathbf{x}}_c^i = \mathbf{x}_c^j) = N(\sum_{l=1}^N \mathbf{w}_c^l)^{-1} \mathbf{w}_c^j$  holds). Consequently, if the resampling mechanism that is employed results

in an ordered list of resampled particles, then a random permutation of the particles indices should be carried out before combining particles from different child populations.

Proposal sampling (Line 2), similarly to standard SMC, is based on user-provided proposal densities  $q_t$ . However, the proposal has access to more information in D&C-SMC, namely to the state of all the children  $c_1, c_2, \dots, c_C$  of node  $t$ :  $q_t(\cdot | \tilde{\mathbf{x}}_{c_1}^i, \dots, \tilde{\mathbf{x}}_{c_C}^i)$ . For each particle tuple  $(\tilde{\mathbf{x}}_{c_1}^i, \dots, \tilde{\mathbf{x}}_{c_C}^i)$  generated in the resampling stage, we sample a successor state  $\tilde{\mathbf{x}}_t^i \sim q_t(\cdot | \tilde{\mathbf{x}}_{c_1}^i, \dots, \tilde{\mathbf{x}}_{c_C}^i)$ . Note that in some cases, parts of the tree structured decomposition do not require this proposal sampling step, namely when  $\tilde{\mathbf{X}}_t = \emptyset$ . We simply set  $\tilde{\mathbf{x}}_t^i$  to  $\emptyset$  in these cases (the resampling and reweighting are still non-trivial).

Finally, we form the  $i$ -th sample at node  $t$  of the tree by concatenating the tuple of resampled child particles  $(\tilde{\mathbf{x}}_{c_1}^i, \dots, \tilde{\mathbf{x}}_{c_C}^i)$  and the proposed state  $\tilde{\mathbf{x}}_t^i$  (if it is non-empty). The importance weight is given by the ratio of the (unnormalised) target densities, divided by the proposal density (Line 2c). We use the convention here that  $\prod_{c \in \emptyset} (\cdot) = 1$ , to take into account the base case of this recursion, at the leaves of the tree.

*Example* (Hierarchical models, continued). A simple choice for  $q_t(\cdot | \tilde{\mathbf{x}}_{c_1}^i, \dots, \tilde{\mathbf{x}}_{c_C}^i)$  in this example is to use  $u_t$ , the (artificial) prior at the sub-tree rooted at node  $\tilde{\mathbf{x}}_t$ . An alternative is to select  $u_t$  as a conjugate prior to the distributions of the children,  $p(\tilde{\mathbf{x}}_c | \tilde{\mathbf{x}}_t)$ ,  $c \in \mathcal{C}(t)$ , and to propose according to the posterior distribution of the conjugate pair. To illustrate the weight update, we show its simplified form in the simplest situation, where  $q_t = u_t$ :

$$\mathbf{w}_t^i = \frac{\gamma_t(\mathbf{x}_t^i)}{\prod_{c \in \mathcal{C}(t)} \gamma_c(\tilde{\mathbf{x}}_c^i)} \frac{1}{q_t(\tilde{\mathbf{x}}_t^i | \tilde{\mathbf{x}}_{c_1}^i, \dots, \tilde{\mathbf{x}}_{c_C}^i)} = \frac{u_t(\mathbf{x}_t^i) \prod_{c \in \mathcal{C}(t)} p(\tilde{\mathbf{x}}_c^i | \tilde{\mathbf{x}}_t^i)}{\prod_{c \in \mathcal{C}(t)} u_c(\tilde{\mathbf{x}}_c^i)} \frac{1}{u_t(\mathbf{x}_t^i)} = \prod_{c \in \mathcal{C}(t)} \frac{p(\tilde{\mathbf{x}}_c^i | \tilde{\mathbf{x}}_t^i)}{u_c(\tilde{\mathbf{x}}_c^i)}.$$

If executed serially, the running time of D&C-SMC is  $O(N \cdot |T|)$ . However, a running time of  $O(N \cdot \text{depth}(T))$  can be achieved via parallelized or distributed computing (see Section 5.3). In terms of memory requirements, they grow at the rate of  $O(N \cdot \text{depth}(T) \cdot \max_t |\mathcal{C}(t)|)$  in the serial case,<sup>1</sup> and at the rate of  $O(N \cdot |T|)$  in the parallel case.<sup>2</sup> Note that the D&C-SMC algorithm generalizes the usual SMC framework; if  $|\mathcal{C}(t)| = 1$  for all internal nodes, then the D&C-SIR procedure described above reduces to a standard SIR method (Algorithm 1).

### 3.3 Theoretical Properties

As D&C-SMC consists of standard SMC steps combined with merging of particle populations via resampling, it is possible (with care) to extend many of the results from the standard, and by now well-studied, SMC setting (see e.g., Del Moral (2004) for a comprehensive collection of theoretical results). Here, we present two results to justify Algorithm 2. The proofs of the two propositions stated below are given in Appendix A.

First of all, the unbiasedness of the normalizing constant estimate of standard SMC algorithms (Del Moral, 2004, Prop. 7.4.1) is inherited by D&C-SMC.

<sup>1</sup>The  $\text{depth}(T)$  factor comes from the maximum size of the recursion stack, and  $N \max_t |\mathcal{C}(t)|$  comes from the requirement for each level of the stack to store a particle population for each child.

<sup>2</sup>In the extreme case where  $|T|/2$  compute nodes are used, one for each leaf of a binary tree.

**Proposition 1.** *Provided that  $\gamma_t \ll \otimes_{c \in \mathcal{C}(t)} \gamma_c \otimes q_t$  for every  $t \in T$  and an unbiased, exchangeable resampling scheme is applied to every population at every iteration, we have for any  $N \geq 1$ :*

$$\mathbb{E}[\widehat{Z}_r] = Z_r = \int \gamma_r(d\mathbf{x}_r).$$

An important consequence of Proposition 1 is that the D&C-SMC algorithm can be used to construct efficient block-sampling MCMC kernels in the framework of particle MCMC Andrieu et al. (2010); see Section 4.3. Our second result shows that the particle system generated by the D&C-SMC procedure is consistent as the number of particles tends to infinity.

**Proposition 2.** *Under regularity conditions detailed in Appendix A.2, the weighted particle system  $(\mathbf{x}_{r,N}^i, \mathbf{w}_{r,N}^i)_{i=1}^N$  generated by `dc.smc`( $r$ ) is consistent in that for all functions  $f : \mathbf{X} \rightarrow \mathbb{R}$  satisfying the assumptions listed in Appendix A.2:*

$$\sum_{i=1}^N \frac{\mathbf{w}_{r,N}^i}{\sum_{j=1}^N \mathbf{w}_{r,N}^j} f(\mathbf{x}_{r,N}^i) \xrightarrow{\mathbb{P}} \int f(\mathbf{x}) \pi(\mathbf{x}) d\mathbf{x}, \quad \text{as } N \rightarrow \infty.$$

### 3.4 Tree structured auxiliary distributions from graphical models

We now present one strategy for building tree structured auxiliary distributions from graphical models. There are other ways of constructing these auxiliary distributions, but for concreteness we focus here on a method targeted at posterior inference for PGMs. On the other hand, the method we present here is more general than it may appear at first: in particular, although the flow of the algorithm follows a tree structure, we do not assume that the graphical models are acyclic.

To illustrate the concepts in this section, we will use two running examples: one coming from a directed PGM, and one coming from an undirected one. We use the factor graph notation from Section 2.2 to introduce the features of these examples salient to the present discussion. We give a more detailed description of the two examples in Section 5.

*Example* (Hierarchical models, continued). Consider a situation where the data is collected according to a known hierarchical structure. For example, test results for an examination are collected by school, which belong to a known school district, which belong to a known county. This situation is similar to the example shown in Figure 3, but where we generalize the number of level to be an arbitrary integer,  $\alpha$ . This yields the factor graph shown in Figure 4(a), where we assume for simplicity a binary structure (this is lifted in Section 5). The nodes in the set  $V$  correspond to latent variables specific to each level of the hierarchy. For example, a variable,  $x_v$ , at a leaf encodes school-specific parameters from a set,  $\tilde{\mathbf{X}}_v$ , those at the second level, district-specific parameters, etc. The set of factors,  $F$ , contain one binary factor,  $\phi(x_v, x_{v'})$ , between each internal node,  $v'$ , and its parent,  $v$ . There is also one factor,  $u_r$ , at the root to encode a top level prior.

*Example* (Lattice models). Two-dimensional regular lattice models such as the Ising model are frequently used in spatial statistics and computer vision to encourage nearby locations in a spatial latent field to take on similar values; see Figure 4(b). We denote the width of

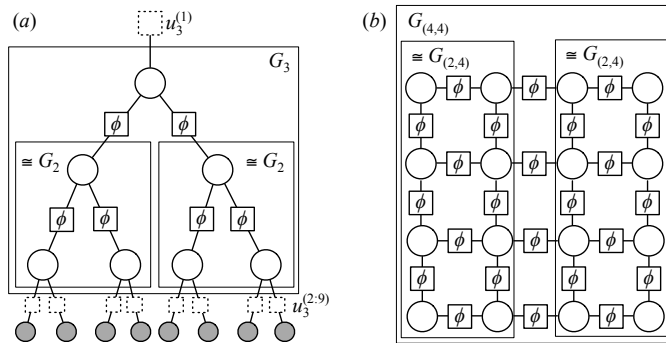


Figure 4: Examples of factor graph families, and self-similarities among them. (a) A hierarchical model for  $\alpha = 3$ . The unaries  $u_\alpha$  consist in a product of 9 individual unary factors: one for the root, and 8 for the leaves (note that the binary factors connected to the 8 observed leaves can be considered as unary factors since one of their arguments is fixed and known for the purpose of posterior inference). Hence,  $|V_3| = 7$ ,  $|F_3| = 6$ ,  $k_\alpha = 2$ ,  $\alpha_1 = \alpha_2 = 2$ . (b) A rectangular lattice model (e.g., an Ising model) for  $\alpha = (4, 4)$ . Here,  $k_\alpha = 2$ ,  $\alpha_1 = \alpha_2 = (2, 4)$ .

the grid by  $\alpha^{(1)}$  and the height by  $\alpha^{(2)}$ . The cardinality of  $V$  is thus  $\alpha^{(1)}\alpha^{(2)}$ . The bivariate factors connect variables with Manhattan distance of one to each other.

Note that the previous two examples actually describe a collection of factor graphs indexed by  $\alpha$ : in the hierarchical model example,  $\alpha$  is a positive integer encoding the number of hierarchical levels; in the lattice model example,  $\alpha$  is a pair of positive integers,  $\alpha = (\alpha^{(1)}, \alpha^{(2)})$  encoding the width and height of the grid. To formalize this idea, we define a *model family* as a collection of factor graphs:  $\mathcal{M} = \{G_\alpha = (V_\alpha, F_\alpha)\}$ , where  $V_\alpha \neq \emptyset$ . Since we would like the concept of model family to encode the model structure rather than some observation-specific configurations, it will be useful in the following to assume that the sets  $F_\alpha$  only contain factors linking at least two nodes. Given  $G_\alpha$  and a dataset, it is trivial to add back the unary factors, denoted  $u_\alpha$ . We assume that for all  $\alpha$ , adding these unary factors to the product of the factors in  $F_\alpha$  yields a model of finite normalization,  $\int u_\alpha \prod_{\phi \in F_\alpha} \phi d\mu < \infty$ .

To build a tree of auxiliary distributions, we rely on a notion of self-similarity. We start with an illustration of what we mean by self-similarity in the two running examples.

*Example* (Hierarchical models, continued). Consider the factor graph  $G_3 = (V_3, F_3)$  corresponding to a three-level hierarchical model. If we exclude the unary factor at the root, we see that  $G_3$  contains  $G_2$  as a subgraph (see Figure 4(a)). In fact,  $G_3$  contains two distinct copies of the graph  $G_2$ .

*Example* (Lattice models, continued). Consider the factor graph  $G_{(4,4)}$  corresponding to a 4-by-4 Ising model (Figure 4(b)). The graph  $G_{(4,4)}$  contains the graph  $G_{(2,4)}$  as a subgraph. Again,  $G_{(4,4)}$  contains in fact two distinct copies of the subgraph.

Formally, we say that a model family is *self-similar*, if given any  $G_\alpha \in \mathcal{M}$  with  $|V_\alpha| > 1$ , we can find  $\alpha_1, \alpha_2, \dots, \alpha_{k_\alpha}, k_\alpha > 1$  such that the disjoint union  $\sqcup_i G_{\alpha_i}$  can be *embedded* in  $G_\alpha$ . By embedding, we mean that there is a one-to-one graph homomorphism from  $\sqcup_i G_{\alpha_i}$  into  $G_\alpha$ . This graph homomorphism should respect the labels of the nodes and edge (i.e. differentiates variable, factors, and the various types of factors).

*Example* (Lattice models, continued). Therefore, if  $|V_\alpha| > 1$ , then at least one of  $\alpha^{(1)}$  or  $\alpha^{(2)}$  is greater than one, let us say the first one without loss of generality. As shown in Figure 4(b), we can therefore pick  $k_\alpha = 2$  and  $\alpha_1 = (\lfloor \alpha^{(1)}/2 \rfloor, \alpha^{(2)})$ ,  $\alpha_2 = (\lceil \alpha^{(1)}/2 \rceil, \alpha^{(2)})$ .

Given a member  $\alpha_0$  of a self-similar model family, there is a natural way to construct a tree decomposition of auxiliary distributions. First, we recursively construct  $T$  from the self-similar model indices: we set  $r = \alpha_0$ , and given any  $t = \alpha \in T$ , we set  $\mathcal{C}(t) \subset T$  to  $\alpha_1, \alpha_2, \dots, \alpha_{k_\alpha}$ .<sup>3</sup> Second, given an index  $t = \alpha \in T$ , we set  $\pi_t$  to  $u_\alpha \prod_{\phi \in F_\alpha} \phi$ . Note that by the embedding property, this choice is guaranteed to satisfy Equation (5), where  $\mathbf{X}_{c_i}$  corresponds to the range of the random vector defined from the indices in  $V_{\alpha_i}$ .

## 4 Extensions

Algorithm 2 is essentially an SIR algorithm and variables are not rejuvenated after their first sampling. Inevitably, as in particle filtering, this will lead to degeneracy as repeated resampling steps reduce the number of unique particles. Techniques employed to ameliorate this problem in the particle filtering literature could be used—fixed lag techniques (Kitagawa, 1996) might make sense in some settings, as could incorporating MCMC moves (Gilks and Berzuini, 2001). In this section we present several extensions to address the degeneracy problem more directly, and we also discuss adaptive schemes for improving the computational efficiency of the proposed method. The extensions presented here comprise fundamental components of the general strategy introduced in this paper, and may be required to obtain good performance in challenging settings.

### 4.1 Merging subpopulations via mixture sampling

The resampling in Step 1b of the `dc.smc` procedure, which combines subpopulations to target a new distribution on a larger space, is critical. The independent multinomial resampling of child populations in the basic D&C-SIR procedure corresponds to sampling  $N$  times with replacement from the product measure (6). The low computational cost of this approach is appealing, but unfortunately it can lead to high variance when the product  $\prod_{c \in \mathcal{C}(t)} \pi_c(\mathbf{x}_c)$  differs substantially from the corresponding marginal of  $\pi_t$ .

An alternative approach, akin to the mixture proposal approach (Carpenter et al., 1999) or the auxiliary particle filter (Pitt and Shephard, 1999), is described below. The idea is to exploit the fact that the product measure has mass upon  $N^{|\mathcal{C}(t)|}$  points, in order to capture the dependencies among the variables in the target distribution  $\pi_t(\mathbf{x}_t)$ . Let  $\tilde{\pi}_t(\mathbf{x}_{c_1}, \dots, \mathbf{x}_{c_C})$  be some distribution which incorporates this dependency (in the simplest case we might take  $\tilde{\pi}_t(\mathbf{x}_{c_1}, \dots, \mathbf{x}_{c_C}) \approx \int \pi_t(\mathbf{x}_{c_1}, \dots, \mathbf{x}_{c_C}, \tilde{\mathbf{x}}_t) d\tilde{\mathbf{x}}_t$  or, when  $\tilde{\mathbf{X}}_t = \emptyset$ ,  $\tilde{\pi}_t \equiv \pi_t$ ; see below for an alternative). We can then replace Step 1b of Algorithm 2 with simulating  $\{(\tilde{\mathbf{x}}_{c_1}^i, \dots, \tilde{\mathbf{x}}_{c_C}^i)\}_{i=1}^N$

---

<sup>3</sup>This recursive process will yield a finite set  $T$ : since  $V_\alpha$  is assumed to be non-empty, it suffices to show that  $|V_{\alpha_i}| < |V_\alpha|$  for all  $i \in \{1, \dots, k_\alpha\}$  whenever  $|V_\alpha| > 1$ . But since  $k_\alpha > 1$ , and that the disjoint union  $\sqcup_i G_{\alpha_i}$  can be embedded in  $G_\alpha$ , it follows that  $|V_\alpha| \geq |V_{\alpha_i}| + \sum_{j \neq i} |V_{\alpha_j}|$ . Since  $|V_{\alpha_j}| > 0$ , the conclusion follows.

from

$$Q_t(d\mathbf{x}_{c_1}, \dots, d\mathbf{x}_{c_C}) := \sum_{i_1=1}^N \dots \sum_{i_C=1}^N \frac{v_t(i_1, \dots, i_C) \delta_{(\mathbf{x}_{c_1}^{i_1}, \dots, \mathbf{x}_{c_C}^{i_C})}(\mathbf{d}\mathbf{x}_{c_1}, \dots, \mathbf{d}\mathbf{x}_{c_C})}{\sum_{j_1=1}^N \dots \sum_{j_C=1}^N v_t(j_1, \dots, j_C)}, \quad (7)$$

$$v_t(i_1, \dots, i_C) := \left( \prod_{c \in \mathcal{C}(t)} \mathbf{w}_c^{i_c} \right) \tilde{\pi}_t(\mathbf{x}_{c_1}^{i_1}, \dots, \mathbf{x}_{c_C}^{i_C}) / \prod_{c \in \mathcal{C}(t)} \pi_c(\mathbf{x}_c^{i_c}),$$

with the weights of Step 2c computed using  $\mathbf{w}_t^i \propto \pi_t(\mathbf{x}_t^i) / [\tilde{\pi}_t(\tilde{\mathbf{x}}_{c_1}^{i_1}, \dots, \tilde{\mathbf{x}}_{c_C}^{i_C}) q_t(\tilde{\mathbf{x}}_t^i | \tilde{\mathbf{x}}_{c_1}^{i_1}, \dots, \tilde{\mathbf{x}}_{c_C}^{i_C})]$ . Naturally, if we take  $\tilde{\pi}_t(\mathbf{x}_{c_1}, \dots, \mathbf{x}_{c_C}) = \prod_{c \in \mathcal{C}(t)} \pi_c(\mathbf{x}_c)$  we recover the basic approach discussed in Section 3.2.

Clearly, the computational cost of simulating from  $Q_t$  will be  $O(N^{|\mathcal{C}(t)|})$ . However, we envisage that both  $|\mathcal{C}(t)|$  and the number of coalescence events (i.e. combinations of sub-populations via this step) are sufficiently small that this is not a problem in many cases. Should it be problematic, computationally efficient use of products of mixture distributions is possible employing the strategy of Briers et al. (2005). At the cost of introducing a small and controllable bias, techniques borrowed from  $N$ -body problems could also be used when dealing with simple local interactions (Gray and Moore, 2001). Furthermore, if the mixture sampling approach is employed it significantly mitigates the impact of resampling, and it is possible to reduce the branching factor by introducing additional (dummy) internal nodes in  $T$ . For example, by introducing additional nodes in order to obtain a binary tree (see Section 5.1), the merging of the child populations will be done by coalescing pairs, then pairs of pairs, etc., gradually taking the dependencies between the variables into account.

## 4.2 SMC samplers and tempering within D&C-SMC

As discussed in Section 2.3, a common strategy when simulating from some complicated distribution using SMC is to construct a synthetic sequence of distributions (3) which moves from something tractable to the target distribution of interest (Del Moral et al., 2006). The SMC proposals can then, for instance, be chosen as MCMC transition kernels—this is the approach that we detail below for clarity.

Step 2 of Algorithm 2 corresponds essentially to a (sequential) importance sampling step. Using the notation introduced in the previous section, we obtain after the resampling/mixture sampling step an unweighted sample  $\{(\tilde{\mathbf{x}}_{c_1}^i, \dots, \tilde{\mathbf{x}}_{c_C}^i)\}_{i=1}^N$  targeting  $\tilde{\pi}_t$ , which is extended by sampling from  $q_t(\tilde{\mathbf{x}}_t | \mathbf{x}_{c_1}, \dots, \mathbf{x}_{c_C})$ , and then re-weighted to target  $\pi_t(\mathbf{x}_t)$ . We can straightforwardly replace this with several SMC sampler iterations, targeting distributions which bridge from  $\pi_{t,0}(\mathbf{x}_t) = \tilde{\pi}_t(\mathbf{x}_{c_1}, \dots, \mathbf{x}_{c_C}) q_t(\tilde{\mathbf{x}}_t | \mathbf{x}_{c_1}, \dots, \mathbf{x}_{c_C})$  to  $\pi_{t,n_t}(\mathbf{x}_t) = \pi_t(\mathbf{x}_t)$ , typically by following a geometric path  $\pi_{t,j} \propto \pi_{t,0}^{1-\alpha_j} \pi_{t,n_t}^{\alpha_j}$  with  $0 < \alpha_1 < \dots < \alpha_{n_t} = 1$ . Step 2 of Algorithm 2 is then replaced by:

- 2'. (a) For  $i = 1$  to  $N$ , simulate  $\tilde{\mathbf{x}}_t^i \sim q_t(\cdot | \tilde{\mathbf{x}}_{c_1}^i, \dots, \tilde{\mathbf{x}}_{c_C}^i)$ .
- (b) For  $i = 1$  to  $N$ , set  $\mathbf{x}_{t,0}^i = (\tilde{\mathbf{x}}_{c_1}^i, \dots, \tilde{\mathbf{x}}_{c_C}^i, \tilde{\mathbf{x}}_t^i)$  and  $\mathbf{w}_{t,0}^i = 1$ .
- (c) For SMC sampler iteration  $j = 1$  to  $n_t$ :
  - i. For  $i = 1$  to  $N$ , compute  $\mathbf{w}_{t,j}^i = \mathbf{w}_{t,j-1}^i \gamma_{t,j}(\mathbf{x}_{t,j-1}^i) / \gamma_{t,j-1}(\mathbf{x}_{t,j-1}^i)$ .

- ii. Optionally, resample  $\{\mathbf{x}_{t,j-1}^i, \mathbf{w}_{t,j}^i\}_{i=1}^N$  and override the notation  $\{\mathbf{x}_{t,j-1}^i, \mathbf{w}_{t,j}^i\}_{i=1}^N$  to refer to the resampled particle system.
- iii. For  $i = 1$  to  $N$ , draw  $\mathbf{x}_{t,j}^i \sim K_{t,j}(\mathbf{x}_{t,j-1}^i, \cdot)$  using a  $\pi_{t,j}$ -reversible Markov kernel  $K_{t,j}$ .
- (d) Set  $\mathbf{x}_t^i = \mathbf{x}_{t,n_t}^i$  and  $\mathbf{w}_t^i = \mathbf{w}_{t,n_t}^i$ .

The computation of normalizing constant estimates has been omitted for brevity, but follows by standard arguments (the complete algorithm is provided in Appendix B).

We believe that the mixture sampling approach (7) can be particularly useful when combined with SMC tempering as described above. Indeed, mixture sampling can be used to enable efficient initialization of each (node-specific) SMC sampler by choosing, for  $\alpha_\star \in [0, 1]$ ,

$$\tilde{\pi}_t(\mathbf{x}_{c_1}, \dots, \mathbf{x}_{c_C}) \propto \left[ \prod_{c \in \mathcal{C}(t)} \pi_c(\mathbf{x}_c) \right]^{1-\alpha_\star} \left[ \int \pi_{t,n_t}(\mathbf{x}_{c_1}, \dots, \mathbf{x}_{c_C}, \tilde{\mathbf{x}}_t) d\tilde{\mathbf{x}}_t \right]^{\alpha_\star}. \quad (8)$$

That is, we exploit the fact that the distribution (7) has support on  $N^{|\mathcal{C}(t)|}$  points to warm-start the annealing procedure at a non-zero value of the annealing parameter  $\alpha_\star$ . In practice, this has the effect that we can typically use fewer temperatures  $n_t$ . In particular, if simulating from the MCMC kernels  $K_{t,j}$  is computationally costly, requiring fewer samples from these kernels can compensate for the  $O(N^{|\mathcal{C}(t)|})$  computational cost associated with (7).

### 4.3 Particle MCMC

The seminal paper by Andrieu et al. (2010) demonstrated that SMC algorithms can be used to produce approximations of idealized block-sampling proposals within MCMC algorithms. By interpreting these particle MCMC algorithms as standard algorithms on an extended space, incorporating all of the variables sampled during the running of these algorithms, they can be shown to be exact, in the sense that the apparent approximation does not change the invariant distribution of the resulting MCMC kernel. Proposition 1, and in particular the construction used in its proof, demonstrates how the class of D&C-SMC algorithms can be incorporated within the particle MCMC framework. Such techniques are now essentially standard, and we do not dwell on this approach here.

### 4.4 Adaptation

Adaptive SMC algorithms have been the focus of much attention in recent years. Del Moral et al. (2012) provides the first formal validation of algorithms in which resampling is conducted only sometimes according to the value of some random quantity obtained from the algorithm itself. We advocate the use of low variance resampling algorithms (Douc et al., 2005, e.g.) to be applied adaptively. Other adaptation is possible within SMC algorithms. Two approaches are analyzed formally by Beskos et al. (2014): the adaptation of the parameters of the MCMC kernels employed (step 2'(c)iii.) and of the number and location of distributions employed within tempering algorithms, i.e.,  $n_t$  and  $\alpha_1, \dots, \alpha_{n_t}$ ; see e.g., Zhou et al. (2015) for one approach to this.



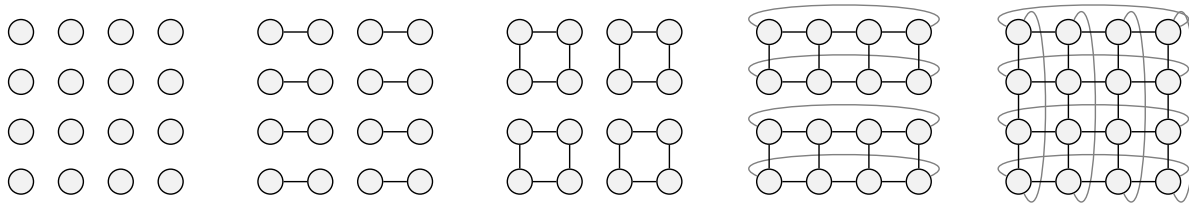


Figure 5: The disconnected components correspond to the groups of variables that are targeted by the different populations of the D&C-SMC algorithm. At the final iteration, corresponding to the rightmost figure, we recover the original, connected model.

Adaptation is especially appealing within D&C-SMC: beyond the usual advantages it allows for the concentration of computational effort on the more challenging parts of the sampling process. Using adaptation will lead to more intermediate distributions for the subproblems (i.e., the steps of the D&C-SMC algorithm) for which the starting and ending distributions are more different. Furthermore, it is also possible to adapt the parameter  $\alpha_*$  in (8)—that is, the starting value for the annealing process—based, e.g., on the effective sample size of the  $N^{|\mathcal{C}^{(t)}|}$  particles comprising (7). In simulations (see Section 5.1) we have found that the effect of such adaptation can result in  $\alpha_* = 1$  for many of the “simple” subproblems, effectively removing the use of tempering when this is not needed and significantly reducing the total number of MCMC simulations.

As a final remark, we have assumed throughout that all particle populations are of size  $N$ , but this is not necessary. Intuitively, fewer particles are required to represent simpler low-dimensional distributions than to represent more complex distributions. Manually or adaptively adjusting the number of particles used within different steps of the algorithm remains a direction for future investigation.

## 5 Experiments

### 5.1 Markov Random Field

One model class for which the D&C-SMC algorithm can potentially be useful are Markov random fields (MRFs). To illustrate this, we consider the well-known square-lattice Ising model: each lattice site is associated with a binary spin variable  $x_k \in \{-1, 1\}$  and the configuration probability is given by  $p(\mathbf{x}) \propto e^{-\beta E(\mathbf{x})}$ , where  $\beta \geq 0$  is the inverse temperature and  $E(\mathbf{x}) = -\sum_{(k,\ell) \in \mathcal{E}} x_k x_\ell$  is the energy of the system. Here,  $\mathcal{E}$  denotes the edge set for the graphical model which we assume correspond to nearest-neighbour interactions with periodic boundary conditions, see Figure 5 (rightmost figure).

Let the lattice size be  $M \times M$ , with  $M$  being a power of 2 for simplicity. To construct the computational tree  $T$  we make use of the strategy of Section 3.4. That is, we start by dividing the lattice into two halves, removing all the edges between them. We then continue recursively, splitting each sub-model in two, until we obtain a collection of  $M^2$  disconnected nodes; see Figure 5. This decomposition of the model defines a binary tree  $T$ , on which the D&C-SMC algorithm operates. At the leaves we initialize  $M^2$  independent particle popu-

lations by sampling uniformly on  $\{-1, 1\}$ . These populations are then resampled, merged, and reweighted as we proceed up the tree, successively reintroducing the “missing” edges of the model (note that  $\mathbf{X}_t = \emptyset$  for all non-leaf nodes  $t$  in this example). This defines the basic D&C-SIR procedure for the MRF. We also consider three extensions of this procedure:

**D&C-SMC (mix)** uses the mixture sampling strategy described in Section 4.1: the edges connecting any two sub-graphs are introduced before the corresponding sub-populations are merged.

**D&C-SMC (ann)** uses the tempering method discussed in Section 4.2: when the edges connecting two sub-graphs are reintroduced this is done gradually according to an annealing schedule to avoid severe particle depletion at the later stages of the algorithm.

**D&C-SMC (mix+ann)** uses both mixture sampling and tempering.

For the annealed methods, we use single-flip Metropolis-Hastings kernels. The annealing schedules are set adaptively based on the conditional ESS (CESS) criterion of Zhou et al. (2015), with CESS threshold 0.995. For D&C-SMC (mix+ann) we warm-start each annealing process by selecting  $\alpha_*$  in (8) based on the CESS (threshold 0.95) in each of the marginals of  $\tilde{\pi}_t(\mathbf{x}_{c_1}, \mathbf{x}_{c_2})$ . We also compare these methods with, (i) a standard SMC sampler with adaptive annealing Del Moral et al. (2006), and (ii) a single-flip Metropolis-Hastings sampler. All methods were implemented in Matlab 8.0.

We consider a grid of size  $64 \times 64$  with  $\beta = 0.4407$  (the critical temperature). We ran the methods listed above with  $N = 2^6$  to  $2^{11}$  particles, with the exception of D&C-SIR which got  $2^{10}$  to  $2^{15}$  particles to more closely match its computational cost with the others’. The single-flip MH sampler was run for  $2^{14}$  MCMC iterations (each iteration being one complete sweep), with the first  $2^{10}$  iterations discarded as burn-in. We ran each method 50 times and considered the estimates of (i) the normalising constant  $Z$  and (ii) the expected value of the energy  $\mathbb{E}[E(\mathbf{x})]$ . The results are given in Figure 6.

D&C-SIR and D&C-SMC (mix) gave inferior results to D&C-SMC (ann) and D&C-SMC (ann+mix) for this model and have therefore been excluded (the results for all methods are given in Appendix C). Among the remaining methods, D&C-SMC (ann) and D&C-SMC (mix+ann) give the overall best performance, significantly outperforming both standard SMC and single flip MH sampling for the same computational time.

For the two D&C-SMC samplers—D&C-SMC (ann) and D&C-SMC (mix+ann)—the performance is comparable. Whether or not it is worthwhile to make use of the mixture sampling strategy (Section 4.1) is likely to be highly problem dependent. The benefit of using mixture sampling is that it can result in that fewer annealing steps need to be taken. Indeed, for the simulations presented above, the SMC sampler used on average (over all different settings and runs) 685 MCMC updates for each site. The corresponding numbers for D&C-SMC (ann) and D&C-SMC (mix+ann) were 334 and 176, respectively. That is, for this example mixture sampling essentially halves the number MCMC iterations that are taken compared to D&C-SMC (ann) (which in turn uses only half the number of MCMC iterations compared to standard SMC). Hence, for models where simulation from the MCMC kernel is computationally expensive it can be worthwhile to use mixture sampling, even though its intrinsic computational cost is  $O(N^2)$ .

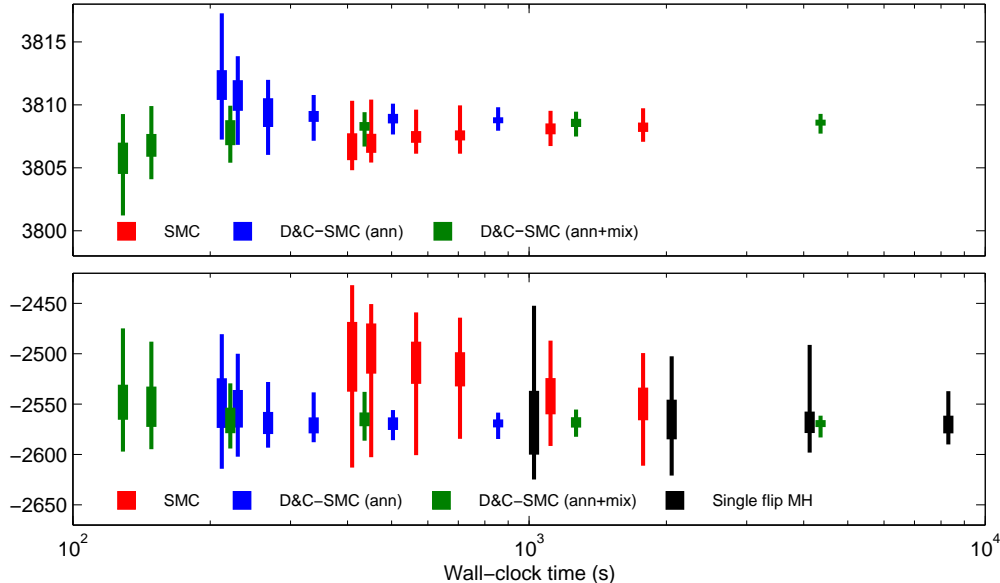


Figure 6: Box-plots (min, max, and inter-quartile) of estimates of  $\log Z$  (top) and  $\mathbb{E}[E(\mathbf{x})]$  (bottom) over 50 runs of each sampler (excluding single flip MH in the top panel since it does not readily provide an estimate of  $\log Z$ ). The boxes, as plotted from left to right, correspond to increasing number of particles  $N$  (or number of MCMC iterations for single flip MH).

The fact that mixture sampling automatically results in more computational effort being spent on the most difficult subproblems can be further illustrated by considering the distribution of values of the parameter  $\alpha_*$  in (8). Recall that  $\alpha_* \in [0, 1]$  is the value of the annealing parameter at which the annealing process is warm-started. In Figure 7 we show the distribution of  $\alpha_*$  for D&C-SMC (mix+ann) with  $N = 2048$  particles (similar distributions were obtained for the other settings as well), at different levels at the computational tree  $T$ . Due to the way  $T$  is constructed, the number of edges that are “added to the model” at the merge steps increases as we move upward in  $T$ . Indeed, for this model the depth of  $T$  is  $2 \log_2(64) + 1 = 13$  and the number of edges that are added during the merge-steps of the 12 non-leaf levels are: 1, 2, 2, 4, 4, 8, 8, 16, 16, 32, 64, 128. For the first five levels of  $T$ , we obtained  $\alpha_* = 1$  for all nodes, meaning that no annealing was performed during these steps of the algorithm (these levels are excluded from the figure). For the subsequent levels we obtained values of  $\alpha_*$  less than 1, as can be seen in Figure 7, but we are still able to warm-start the annealing at a non-zero value, effectively reducing the number of annealing steps that needs to be taken.

In Appendix C we report additional numerical results for the Ising model (different temperatures) as well as for another square-lattice MRF model with continuous latent variables and a multimodal posterior. These additional results are in general agreement with the ones presented here.

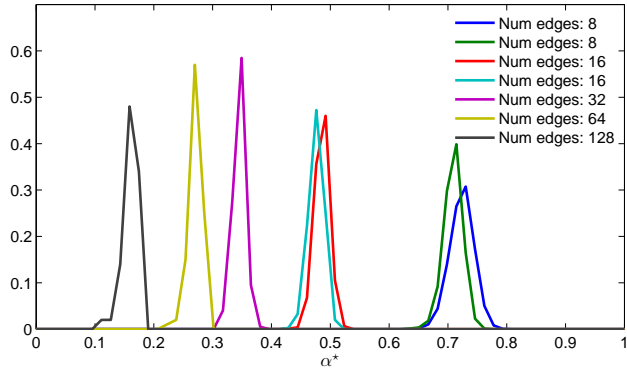


Figure 7: Distributions of  $\alpha_*$  for the merge-steps at the 7 top-most levels of  $T$  (computed for all nodes and over all 50 runs) for D&C-SMC (mix+ann) with 2048 particles.

## 5.2 Hierarchical Bayesian Model – New York State Mathematics Test

In this section, we demonstrate the scalability of our method by analysing a dataset containing *New York State Mathematics Test* results for elementary and middle schools.

### Data and model

After preprocessing (data acquisition and preprocessing are described in detail in Appendix D), we organize the data into a tree  $T$ . A path from the root to a leaf has the following form: NYC (the root, denoted by  $r \in T$ ), borough, school district, school, year. Each leaf  $t \in T$  comes with an observation of  $m_t$  exam successes out of  $M_t$  trials. There were a total of 278 399 test instances in the dataset, split across five borough (Manhattan, The Bronx, Brooklyn, Queens, Staten Island), 32 distinct districts, and 710 distinct schools.

We use the following model, based on standard techniques from multi-level data analysis (Gelman and Hill, 2006). The number of successes  $m_t$  at a leaf  $t$  is assumed to be binomially distributed, with success probability parameter  $p_t = \text{logistic}(\theta_t)$ , where  $\theta_t$  is a latent parameter. Moreover, we attach latent variables  $\theta_t$  to internal nodes of the tree as well, and model the difference in values along an edge  $e = (t \rightarrow t')$  of the tree with the following expression:  $\theta_{t'} = \theta_t + \Delta_e$ , where,  $\Delta_e \sim N(0, \sigma_e^2)$ . We put an improper prior (uniform on  $(-\infty, \infty)$ ) on  $\theta_r$ .<sup>4</sup> We also make the variance random, but shared across siblings,  $\sigma_e^2 = \sigma_t^2 \sim \text{Exp}(1)$ .

### D&C SMC implementation

We apply the basic D&C-SIR to this problem, using the natural hierarchical structure provided by the model (see Section 3.4). Note that conditionally on values for  $\sigma_t^2$  and for the  $\theta_t$  at the leaves, the other random variables are multivariate normal. Therefore, we instantiate values for  $\theta_t$  only at the leaves, and when proposing at an internal node  $t'$ , we only need to propose a value for  $\sigma_{t'}^2$  as the internal parameters  $\theta_{t'}$  can be analytically marginalized conditionally on  $\sigma_{t'}^2$  and  $\theta_{t'}$  using a simple message passing algorithm.

<sup>4</sup>When  $m_t \notin \{0, M_t\}$  for at least one leaf, this can be easily shown to yield a proper posterior.

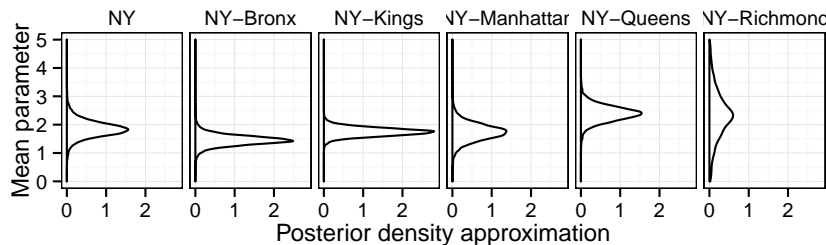


Figure 8: Posterior densities for the parameters  $\theta_t$  with D&C-SIR ran with 10 000 particles. The values of the internal  $\theta_t$  are marginalized during inference, but can be easily reinstated from the samples as a post-processing step.

Each step of D&C-SMC therefore falls in exactly one of two cases: (i) At the leaves we propose a value for  $p_t$  from a Beta distribution with parameters  $1+m_t$  and  $1+M_t-m_t$ , which we map deterministically to  $\theta_t = \text{logit}(p_t)$ . The corresponding weight update is a constant. (ii) At the internal nodes we propose  $\sigma_t^2 \sim \text{Exp}(1)$  from its prior. The weight update ratio involves the densities of marginalized multivariate normal distributions which can be computed efficiently using message passing. Our Java implementation is open source and can be adapted to other multilevel Bayesian analysis scenarios. The code and scripts used to perform our experiments are available at <https://github.com/alexandrebourchard/multilevelSMC>.

The qualitative results obtained from DC with 10 000 particles (Figure 8) are in broad agreement with other socio-economic indicators. For example, among the five counties corresponding to each of the five boroughs, Bronx County has the highest fraction (41%) of children (under 18) living below poverty level.<sup>5</sup> Queens has the second lowest (19.7%), after Richmond (Staten Island, 16.7%). However the fact that Staten Island contains a single school district means that our posterior distribution is much flatter for this borough.

## Comparison of posterior inference methods

For the purpose of comparison, we also applied three additional methods

**Gibbs:** A Metropolis-within-Gibbs algorithm, proposing a change on a single variable using a normal proposal of unit variance. As with D&C-SIR, we marginalize the internal  $\theta_t$  parameters. (Java implementation.)

**STD:** A standard (single population) bootstrap filter with the intermediate distributions being sub-forests incrementally built in post-order. The internal  $\theta_t$ -parameters are marginalized. (Java implementation.)

**Stan:** An open-source implementation of the Hamiltonian Monte Carlo algorithm (see, e.g., Neal (2011)). We did not implement marginalization of the internal  $\theta_t$ -parameters. Stan includes a Kalman inference engine, however it is limited to chain-shaped PGMs as of version 2.6.0. (C++ implementation.)

<sup>5</sup>Statistics from the New York State Poverty Report 2013, <http://ams.nyscommunityaction.org/Resources/Documents/News/>

Further details on the baselines and the experimental setup can be found in Appendix D.

We measure efficiency using effective sample size (ESS) per minute, as well as convergence of the posterior distributions on the parameters. For the MCMC methods (Gibbs and Stan), the ESS is estimated using the standard auto-regressive method, as implemented by Plummer et al. (2006). For the SMC methods (D&C-SMC and STD), the non-sequential nature of the samples dictates a different estimator, hence, again following standard practices, we use the estimator described by Kong et al. (1994). For both MCMC and SMC methods, wall-clock time is measured on Intel Xeon E5430 quad-core processors, running at 2.66 GHz. We replicated all running-time experiments ten times.

We begin with the ESS per minute results for the SMC methods ran with 10 000 particles. For D&C-SMC, we obtained a mean ESS/min of 636.8 (19.3), and for STD, of 537.8 (53.2). The diagnostics suggest that both methods perform reasonably well, with a slight advantage to D&C-SMC. In contrast, the MCMC diagnostics raised inefficiency concerns. For Gibbs (300 000 iterations), we obtained a mean ESS/min of 0.215 (standard deviation of 0.010). The performance of Stan (20 000 iterations) was inferior, and more volatile, with a mean of 0.000848 (0.0016). We attribute the poor performance of the Stan baseline to the fact that it does not marginalize the parameters  $\theta$  (the reason for this is explained in the previous section).

Since the different types of samples impose the use of two different ESS estimators, direct comparisons of ESS/min between an SMC and an MCMC method should be taken with a pinch of salt. However, these results show that the sampling problem we are investigating in this section is indeed a challenging one. This is not a surprise, given the high-dimensionality of the latent variables (3 555 remaining parameters after marginalization of the multivariate normal). Moreover, our results on the convergence of the posterior distributions on the parameters recapitulate that *(i)* the SMC methods strongly outperform the MCMC baselines in this problem, and *(ii)* D&C-SMC and STD perform similarly, with a slight advantage for D&C-SMC. Additional results supporting this claim can be found in Appendix D.

Next, to better differentiate the two SMC methods, we investigate estimation of the log-normalizing constant  $\log(Z)$ . The results are shown in Figure 9. Since there is little change between the D&C-SMC estimate with 100k and 1M particles ( $-3811.60(0.80)$  and  $-3811.15(0.33)$  respectively), it is reasonable to assume that the true negative log-normalization is in the range 3 811–3 812. Under this assumption, D&C-SMC outperforms STD on all computational budgets. Note that the abscissa is in logscale, suggesting that in the large computational budgets, D&C-SMC requires roughly one order of magnitude less particles than STD to reach a similar accuracy. These results have practical implications to situations where particle MCMC is required. Indeed, in the light of Doucet et al. (2014), where the authors recommend a standard deviation of the log-likelihood estimator in the range of 1–1.7, around 10 000 particles would be sufficient in the case of D&C-SMC (standard deviation for 10 000 particles is 1.7), whereas closer to 100 000 particles would be needed in the case of STD (standard deviation for 10 000 particles is 2.5).

### 5.3 Distributed Divide-and-Conquer

To demonstrate the suitability of D&C-SMC to distributed computing environments, we have implemented a proof-of-concept distributed D&C-SMC algorithm. The main idea in

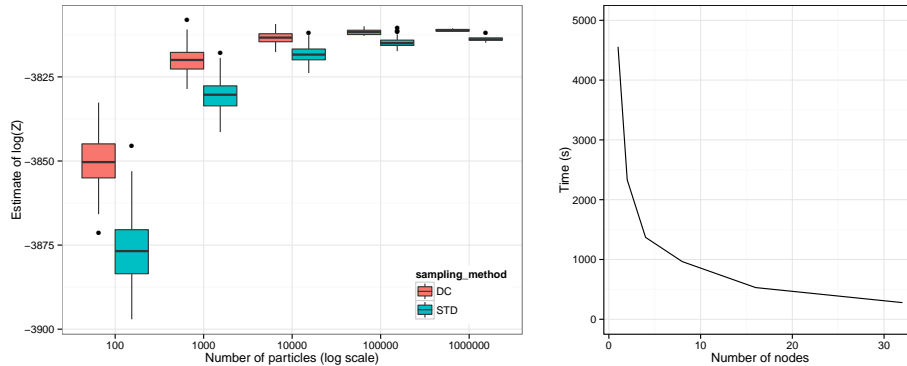


Figure 9: Left: Estimates of  $\log(Z)$  obtained using D&C-SMC and STD with different numbers of particles. Each experiment was replicated 110 times (varying the Monte Carlo seed), except for the experiments with 1M particles, which were replicated only 10 times. Right: Wall-clock times for the distributed D&C-SMC algorithm. See Appendix D for speed-up results.

this implementation is to split the work at the granularity of populations, instead of the more standard particle granularity. The description and benchmarking of this implementation can be found in Appendix D. Using this distributed implementation, we see for example (Figure 9, right) that the running time for 100 000 particles can be reduced from 4 557 seconds for one machine (about  $1\frac{1}{4}$  hours), to 279 seconds (less than five minutes) using 32 compute nodes (each using a single thread).

## 6 Discussion

We have shown that trees of auxiliary distribution can be leveraged by D&C-SMC samplers to provide computationally efficient approximations of the posterior distribution of high-dimensional and possibly loopy probabilistic graphical models. Our method, which generalizes the SMC framework, is additionally easy to distribute across several compute nodes.

As with standard SMC (and other advanced computational inference methods) D&C-SMC allows for a large degree of flexibility, and the method should be viewed as a toolbox rather than as a single algorithm. Indeed, we have discussed several possible extensions of the basic method, and their utility is problem-specific. Furthermore, the interplay between these extensions needs to be taken into account. In particular, based on the numerical results in Section 5.1 we argue that mixture sampling can be useful when used in conjunction with MCMC-based tempering, especially when simulating from the MCMC kernel is computationally costly. In such scenarios, the warm-starting of the tempering process enabled by mixture sampling can compensate for the polynomial (in the branching factor of the tree) computational cost of mixture sampling.

We have assumed in this work that the topology of the tree of auxiliary distributions is known and fixed. In practice, several different decompositions are possible. We have presented one systematic way of obtaining a tree decomposition for self-similar graphical models. However, a natural question to ask is how to choose an optimal decomposition.

We are exploring several approaches to address this question, including strategies that mix several decompositions. How the components of these mixtures should interact is a question we leave for future work.

## References

- Andrieu, C., Doucet, A., and Holenstein, R. (2010). Particle Markov chain Monte Carlo methods. *Journal of the Royal Statistical Society: Series B*, 72(3):269–342.
- Besag, J. (1974). Spatial interaction and the statistical analysis of lattice structures (with discussion). *Journal of the Royal Statistical Society: Series B*, 36:192–236.
- Beskos, A., Jasra, A., Kantas, N., and Thiéry, A. H. (2014). On the convergence of adaptive sequential Monte Carlo algorithms. arxiv, arxiv:1306.6462v3.
- Bishop, C. (2006). *Pattern Recognition and Machine Learning*. Springer.
- Bolic, M., Djuric, P. M., and Hong, S. (2005). Resampling algorithms and architectures for distributed particle filters. *IEEE Transactions on Signal Processing*, 53(7):2442–2450.
- Bouchard-Côté, A., Sankararaman, S., and Jordan, M. I. (2012). Phylogenetic inference via sequential Monte Carlo. *Systematic Biology*, 61(4):579–593.
- Briers, M., Doucet, A., and Maskell, S. (2010). Smoothing algorithms for state-space models. *Annals of the Institute of Statistical Mathematics*, 62(1):61–89.
- Briers, M., Doucet, A., and Singh, S. S. (2005). Sequential auxiliary particle belief propagation. In *Proceedings of the 8th International Conference on Information Fusion*, PA, USA.
- Carpenter, J., Clifford, P., and Fearnhead, P. (1999). Improved particle filter for nonlinear problems. *IEE Proceedings Radar, Sonar and Navigation*, 146(1):2–7.
- Chopin, N. (2002). A sequential particle filter method for static models. *Biometrika*, 89(3):539–551.
- Del Moral, P. (2004). *Feynman-Kac Formulae - Genealogical and Interacting Particle Systems with Applications*. Probability and its Applications. Springer.
- Del Moral, P., Doucet, A., and Jasra, A. (2006). Sequential Monte Carlo samplers. *Journal of the Royal Statistical Society: Series B*, 68(3):411–436.
- Del Moral, P., Doucet, A., and Jasra, A. (2012). On adaptive resampling procedures for sequential Monte Carlo methods. *Bernoulli*, 18(1):252–278.
- Douc, R., Cappé, O., and Moulines, E. (2005). Comparison of resampling schemes for particle filters. In *Proceedings of the 4th IEEE International Symposium on Image and Signal Processing and Analysis*, pages 64–69, Zagreb, Croatia.
- Douc, R. and Moulines, E. (2008). Limit theorems for weighted samples with applications to sequential Monte Carlo. *The Annals of Statistics*, 36(5):2344–2376.
- Doucet, A. and Johansen, A. M. (2011). A tutorial on particle filtering and smoothing. In Crisan, D. and Rozovskii, B., editors, *The Oxford Handbook of Nonlinear Filtering*. OUP.
- Doucet, A., Pitt, M. K., Deligiannidis, G., and Kohn, R. (2014). Efficient implementation of Markov chain Monte Carlo when using an unbiased likelihood estimator. arXiv.org, arXiv:1210.1871v3.



- Gelman, A. and Hill, J. (2006). *Data Analysis Using Regression and Multilevel/Hierarchical Models*. CUP.
- Geweke, J. (2004). Getting it right. *Journal of the American Statistical Association*, 99(467):799–804.
- Gilks, W. R. and Berzuini, C. (2001). Following a moving target – Monte Carlo inference for dynamic Bayesian models. *Journal of the Royal Statistical Society. Series B*, 63(1):127–146.
- Gray, A. G. and Moore, A. W. (2001). 'N-body' problems in statistical learning. In Leen, T. K., Dietterich, T. G., and Tresp, V., editors, *Advances in Neural Information Processing Systems (NIPS) 13*. MIT Press.
- Hoffman, M. and Gelman, A. (2012). The No-U-Turn sampler: Adaptively setting path lengths in Hamiltonian Monte Carlo. *Journal of Machine Learning Research*.
- Jasra, A., Doucet, A., Stephens, D. A., and Holmes, C. C. (2008). Interacting sequential Monte Carlo samplers for trans-dimensional simulation. *Computational Statistics and Data Analysis*, 52(4):1765–1791.
- Jun, S., Wang, L., and Bouchard-Côté, A. (2012). Entangled Monte Carlo. In *Advances in Neural Information Processing Systems 25 (NIPS)*, volume 25, pages 2735–2743.
- Kitagawa, G. (1996). Monte Carlo filter and smoother for non-Gaussian nonlinear state space models. *Journal of Computational and Graphical Statistics*, 5(1):1–25.
- Koller, D., Lerner, U., and Angelov, D. (1999). A general algorithm for approximate inference and its application to hybrid Bayes nets. In *Conference on Uncertainty in Artificial Intelligence (UAI)*, volume 15, pages 324–333.
- Kong, A., Liu, J. S., and Wong, W. H. (1994). Sequential imputations and Bayesian missing data problems. *Journal of the American Statistical Association*, 89(425):278–288.
- Lakshminarayanan, B., Roy, D. M., and Teh, Y. W. (2013). Top-down particle filtering for Bayesian decision trees. In *Proceedings of the 30th International Conference on Machine Learning*, Atlanta, GA, USA.
- Lee, A. and Whiteley, N. (2014). Forest resampling for distributed sequential Monte Carlo. arXiv.org, arXiv:1406.6010.
- Naesseth, C. A., Lindsten, F., and Schön, T. B. (2014). Sequential Monte Carlo for graphical models. In *Advances in Neural Information Processing Systems (NIPS) 27*, pages 1862–1870.
- Neal, R. M. (2001). Annealed importance sampling. *Statistics and Computing*, 11(2):125–139.
- Neal, R. M. (2011). MCMC using Hamiltonian dynamics. In Brooks, S., Gelman, A., Jones, G. L., and Meng, X.-L., editors, *Handbook of Markov Chain Monte Carlo*, pages 113–162. Chapman & Hall/CRC.
- Pearl, J. (1985). Bayesian networks: A model of self-activated memory for evidential reasoning. In *Proceedings of the 7th Conference of the Cognitive Science Society*, pages 329–334, University of California, Irvine, CA, USA. Cognitive Science Society.
- Pitt, M. K. and Shephard, N. (1999). Filtering via simulation: Auxiliary particle filters. *Journal of the American Statistical Association*, 94(446):590–599.
- Plummer, M., Best, N., Cowles, K., and Vines, K. (2006). Coda: Convergence diagnosis and output analysis for mcmc. *R News*, 6(1):7–11.
- Rebeschini, P. and van Handel, R. (2013). Can local particle filters beat the curse of dimensionality? arXiv.org, arXiv:1301.6585.
- Sudderth, E. B., Ihler, A. T., Isard, M., Freeman, W. T., and Willsky, A. S. (2010). Nonparametric belief propagation. *Communications of the ACM*, 53(10):95–103.

- Teh, Y. W., Daumé III, H., and Roy, D. (2008). Bayesian agglomerative clustering with coalescents. In *Advances in Neural Information Processing Systems (NIPS) 20*, pages 1473–1480. MIT Press.
- Vergé, C., Dubarry, C., Del Moral, P., and Moulines, E. (2014). On parallel implementation of sequential monte carlo methods: the island particle model. *Statistics and Computing*. In press.
- Whiteley, N., Lee, A., and Heine, K. (2015). On the role of interaction in sequential Monte Carlo algorithms. *Bernoulli*. In press.
- Zhou, Y., Johansen, A. M., and Aston, J. A. D. (2015). Towards automatic model comparison: An adaptive sequential Monte Carlo approach. *Journal of Computational and Graphical Statistics*. In press.

## A Theoretical Properties

### A.1 Proof of Proposition 1

We consider all of the random variables simulated in the running of the algorithm, following the approach of Andrieu et al. (2010) for standard SIR algorithms. A direct argument provides for the unbiasedness of the normalizing constant estimate by demonstrating that the ratio  $\widehat{Z}_r/Z_r$  is equal to the Radon-Nikodým derivative of a particular extended target distribution to the joint sampling distribution of all of the random variables generated during the running of the algorithm (and is hence of unit expectation).

We provide explicit details for the case in which  $T$  is a balanced binary tree (i.e.  $|\mathcal{C}(t)| = 2$  for every non-leaf node). The more general case follows by the same argument *mutatis mutandis*. We note in particular that the extension to balanced trees of degree greater than two is trivial and that unbalanced trees may be addressed by the introduction of trivial dummy nodes (or directly, at the expense of further complicating the notation).

We assume that subpopulation  $h$  at depth  $d$  is obtained from subpopulations  $2h - 1$  and  $2h$  at depth  $d + 1$ . Let,

$$\mathbf{x}_{\langle D \rangle_2}^{1:N} := \{\mathbf{x}_{(d,h)}^i : (d, h) \in \langle D \rangle_2, i \in \{1, \dots, N\}\}$$

be the collection containing  $N$  particles within each sub-population and let

$$\mathbf{a}_{\langle D \rangle'_2}^{1:N} := \{\mathbf{a}_{(d,h)}^i : (d, h) \in \langle D \rangle'_2, i \in \{1, \dots, N\}\}$$

be the ancestor indices associated with the resampling step;  $\mathbf{a}_{(d,h)}^i$  is the ancestor of the  $i^{\text{th}}$  particle obtained in the resampling step associated with subpopulation  $h$  at level  $d$  of the tree.

First we specify sets in which multi-indices of particle populations live:

$$\langle D \rangle_2 = \bigcup_{d=0}^D \{d\} \otimes \{1, \dots, 2^d\}, \quad \langle D \rangle'_2 = \langle D \rangle_2 \setminus \{0\} \otimes \{1\}.$$

Thus, population  $h$  at depth  $d$ , where the root of the tree is at a depth of 0, may be identified as  $(d, h) \in \langle D \rangle_2$  for any  $d \in \{0, \dots, D\}$ .

The joint distribution from which variables are simulated during the running of the algorithm may be written as:

$$\begin{aligned} \tilde{q} \left( d\mathbf{x}_{\langle D \rangle_2}^{1:N}, d\mathbf{a}_{\langle D \rangle'_2}^{1:N} \right) &= \prod_{h=1}^{2^D} \prod_{i=1}^N q_{(D,h)}(d\mathbf{x}_{(D,h)}^i) \times \prod_{(d,h) \in \langle D \rangle'_2} \prod_{i=1}^N \mathbf{W}_{(d,h)}^{\mathbf{a}_{(d,h)}^i} d\mathbf{a}_{(d,h)}^i \\ &\times \prod_{(d,h) \in \langle D \rangle_2} \prod_{i=1}^N \delta \left( \begin{matrix} \mathbf{a}_{(d+1,2h-1)}^i, \mathbf{a}_{(d+1,2h)}^i \\ \mathbf{x}_{(d+1,2h-1)}^i, \mathbf{x}_{(d+1,2h)}^i \end{matrix} \right) (d(\mathbf{x}_{(d,h)}^i \setminus \tilde{\mathbf{x}}_{(d,h)}^i)) q_{(d,h)}(d\tilde{\mathbf{x}}_{(d,h)}^i | \mathbf{x}_{(d,h)}^i \setminus \tilde{\mathbf{x}}_{(d,h)}^i) \end{aligned}$$

where  $\mathbf{W}_{(d,h)}^i$  denotes the normalized (to sum to one within the realized sample) importance weight of particle  $i$  in subpopulation  $h$  of depth  $d$ . Note that this distribution is over  $(\otimes_{(d,h) \in \langle D \rangle_2} \mathbf{X}_{(d,h)})^N \otimes \{1, \dots, N\}^{|\langle D \rangle'_2|N}$  and the  $d\mathbf{a}$  corresponds to a counting measure over the index set. The inclusion of the singular transition emphasizes the connection between this algorithm and the standard SIR algorithm.

It is convenient to define ancestral *trees* for our particles using the following recursive definition:

$$b_{(0,1)}^i = i \quad \text{and} \quad b_{(d,h)}^i = \begin{cases} b_{(d-1,(h+1)/2)}^i & d \text{ odd,} \\ \mathbf{a}_{(d,h)}^{b_{(d-1,h/2)}^i} & d \text{ even,} \end{cases}$$

the intention being that  $\{b_{(d,h)}^i : (d,h) \in \langle D \rangle'_2\}$  contains the multi-indices of all particles which are ancestral to the  $i^{\text{th}}$  particle at the root.

It is also useful to define an auxiliary distribution over all of the sampled variables and an additional variable  $k$  which indicates a selected ancestral tree from the collection of  $N$ , just as in the particle MCMC context. Here we recall that  $\pi_r = \gamma_r / Z_r$ :

$$\begin{aligned} \tilde{\pi}_r \left( d\mathbf{x}_{\langle D \rangle_2}^{1:N}, d\mathbf{a}_{\langle D \rangle'_2}^{1:N}, dk \right) &= \frac{\pi_r(d\mathbf{x}_{(0,1)}^k) \prod_{(d,h) \in \langle D \rangle_2} \delta_{\mathbf{x}_{(d,h)}^{b_{(d,h)}^k} \setminus \tilde{\mathbf{x}}_{(d,h)}^{b_{(d,h)}^k}} \left( d \left( \mathbf{x}_{(d+1,2h-1)}^{b_{(d+1,2h-1)}^k}, \mathbf{x}_{(d+1,2h)}^{b_{(d+1,2h)}^k} \right) \right)}{N^{|\langle D \rangle_2|}} \\ &\times \frac{\tilde{q} \left( d\mathbf{x}_{\langle D \rangle_2}^{1:N}, d\mathbf{a}_{\langle D \rangle'_2}^{1:N} \right)}{\prod_{h=1}^{2^D} q_{(D,h)}(d\mathbf{x}_{(D,h)}^{b_{(D,h)}^k} \left( \prod_{(d,h) \in \langle D \rangle'_2} \mathbf{W}_{(d,h)}^{b_{(d,h)}^k} \right) \prod_{(d,h) \in \langle D \rangle_2} q_{(d,h)}(d\tilde{\mathbf{x}}_{(d,h)}^{b_{(d,h)}^k} | \mathbf{x}_{(d,h)}^{b_{(d,h)}^k} \setminus \tilde{\mathbf{x}}_{(d,h)}^{b_{(d,h)}^k})} \\ &\times \left( \prod_{(d,h) \in \langle D \rangle_2} \delta \left( \begin{matrix} b_{(d+1,2h-1)}^k, b_{(d+1,2h)}^k \\ \mathbf{x}_{(d+1,2h-1)}^k, \mathbf{x}_{(d+1,2h)}^k \end{matrix} \right) \left( d \left( \mathbf{x}_{(d,h)}^{b_{(d,h)}^k} \setminus \tilde{\mathbf{x}}_{(d,h)}^{b_{(d,h)}^k} \right) \right) \right)^{-1} dk \end{aligned}$$

which can be straightforwardly established to be a properly-normalized probability. Note that the division by a product of singular measures should be interpreted simply as removing the corresponding singular component of the numerator.

Augmenting the proposal distribution with  $k \in \{1, \dots, N\}$  obtained in the same way is convenient (and does not change the result which follows as  $\hat{Z}$  does not depend upon  $k$ ):

$$\bar{q} \left( d\mathbf{x}_{\langle D \rangle_2}^{1:N}, d\mathbf{a}_{\langle D \rangle'_2}^{1:N}, dk \right) = \tilde{q} \left( d\mathbf{x}_{\langle D \rangle_2}^{1:N}, d\mathbf{a}_{\langle D \rangle'_2}^{1:N} \right) \mathbf{W}_{(0,1)}^k dk.$$

It is straightforward to establish that  $\tilde{\pi}_r$  is absolutely continuous with respect to  $\bar{q}$ . Taking the Radon-Nikodým derivative yields the following useful result (the identification between  $\mathbf{x}_{(0,1)}^k$  and its ancestors is taken to be implicit for notational simplicity; as this equality holds with probability one under the proposal distribution, this is sufficient to define the quantity of interest almost everywhere). We allow  $\pi_r$  and  $q_{d,h}$  to denote the *densities* of the measures which they correspond to (with respect to an appropriate version of Lebesgue or counting measure)

$$\begin{aligned} & \frac{d\tilde{\pi}_r}{d\bar{q}} \left( \mathbf{x}_{\langle D \rangle_2}^{1:N}, \mathbf{a}_{\langle D \rangle_2}^{1:N}, k \right) \\ &= \frac{\pi_r \left( \mathbf{x}_{(0,1)}^k \right)}{N^{|\langle D \rangle_2|}} \frac{1}{\prod_{h=1}^{2^D} q_{(D,h)}(\mathbf{x}_{(D,h)}^{b_{(D,h)}^k}) \prod_{(d,h) \in \langle D \rangle_2} q_{(d,h)}(\tilde{\mathbf{x}}_{(d,h)}^{b_{(d,h)}^k} | \mathbf{x}_{(d,h)}^{b_{(d,h)}^k} \setminus \tilde{\mathbf{x}}_{(d,h)}^{b_{(d,h)}^k}) \prod_{(d,h) \in \langle D \rangle_2} \mathbf{W}_{(d,h)}^{b_{(d,h)}^k}} \\ &= \frac{\pi_r \left( \mathbf{x}_{(0,1)}^k \right)}{\prod_{h=1}^{2^D} q_{(D,h)}(\mathbf{x}_{(D,h)}^{b_{(D,h)}^k}) \prod_{(d,h) \in \langle D \rangle_2} q_{(d,h)}(\tilde{\mathbf{x}}_{(d,h)}^{b_{(d,h)}^k} | \mathbf{x}_{(d,h)}^{b_{(d,h)}^k} \setminus \tilde{\mathbf{x}}_{(d,h)}^{b_{(d,h)}^k}) \prod_{(d,h) \in \langle D \rangle_2} \frac{\mathbf{w}_{(d,h)}^{b_{(d,h)}^k}}{\frac{1}{N} \sum_{i=1}^N \mathbf{w}_{(d,h)}^i}} \end{aligned}$$

where  $\mathbf{w}_{(d,h)}^i$  denotes the *unnormalized* importance weight of particle  $i$  in subpopulation  $h$  at depth  $d$ .

We can then identify the product  $\prod_{(d,h) \in \langle D \rangle_2} \mathbf{w}_{(d,h)}^{b_{(d,h)}^k}$  with the ratio of density  $\pi_r$  to the assorted proposal densities evaluated at the appropriate ancestors of the surviving particle multiplied by the normalizing constant  $Z_r$  (by construction; these are exactly the unnormalized weights). Furthermore, we have that

$$\prod_{(d,h) \in \langle D \rangle_2} \frac{1}{N} \sum_{i=1}^N \mathbf{w}_{(d,h)}^i = \hat{Z}_r$$

which implies that  $\tilde{\pi}_r = (\hat{Z}_r/Z_r)\bar{q}$ . Consequently, we obtain the result as:

$$\mathbb{E}_{\bar{q}}[\hat{Z}_r] = \mathbb{E}_{\bar{q}}[Z_r \tilde{\pi}_r / \bar{q}] = Z_r \mathbb{E}_{\tilde{\pi}_r}[1] = Z_r.$$

□

## A.2 Consistency – Proof of Proposition 2

We now turn to consistency. We make a few amendments to the notation used in the main text. First, as we consider limits in the number of particles  $N$ , we add an index  $N$  the particles and their weights. Second, as in the preceding proof we use  $\mathbf{W}$  to denote the normalized weights. For simplicity we also assume a perfect binary tree,  $\mathcal{C}(t) = (t_1, t_2)$ , where  $t_1$  and  $t_2$  denote the left and right children of node  $t$ . The proof in this case captures the essential features of the general case. We base our argument on Douc and Moulines (2008) (henceforth, DM08). We will use the following definitions and assumptions.

1. We require that the Radon-Nikodým derivative

$$\frac{d\gamma_t}{d\gamma_{t_1} \otimes \gamma_{t_2} \otimes q_t}(\mathbf{x}_{t_1}, \mathbf{x}_{t_2}, \tilde{\mathbf{x}}_t) < \infty, \quad (9)$$

is well-defined and finite almost everywhere.

2. We define  $\mathbf{C}_t$  to denote the collection of bounded integrable test function as in DM08.

3. We also make the following assumption (which could be relaxed and which is too strong to cover some of the algorithms and applications discussed in the main text, but which simplifies exposition): there exists a constant  $C$  such that for all  $t, \mathbf{x}_{t_1}, \mathbf{x}_{t_2}, \tilde{\mathbf{x}}_t$ :

$$\frac{d\gamma_t}{d\gamma_{t_1} \otimes \gamma_{t_2} \otimes q_t}(\mathbf{x}_{t_1}, \mathbf{x}_{t_2}, \tilde{\mathbf{x}}_t) < C,$$

4. Assume multinomial or residual resampling is performed at every step.

**Proposition 3.** *Under the above assumptions, the normalized weighted particles  $(\mathbf{x}_N^i, \mathbf{W}_N^i : i \in \{1, \dots, N\})$ ,  $\mathbf{W}_N^i = \mathbf{w}_N^i / \sum_j \mathbf{w}_N^j$ , obtained from `dc_smc`( $r$ ) are consistent with respect to  $(\pi, \mathbf{C}_r)$ , i.e.: for all test function  $f \in \mathbf{C}_r$ , as the number of particles  $N \rightarrow \infty$ :*

$$\sum_{i=1}^N \mathbf{W}_N^i f(\mathbf{x}_N^i) \xrightarrow{\mathbb{P}} \int f(\mathbf{x}) \pi(d\mathbf{x}).$$

**Lemma 1.** *Let  $\mathcal{F}$  denote a  $\sigma$ -algebra generated by a semi-ring  $\mathcal{A}$ ,  $\mathcal{F} = \sigma(\mathcal{A})$ . Let  $\pi$  be a finite measure constructed using a Carathéodory extension based on  $\mathcal{A}$ . Then, given  $\epsilon > 0$  and  $E \in \mathcal{F}$ , there is a finite collection of disjoint simple sets  $R_1, \dots, R_n$  that cover  $E$  and provide an  $\epsilon$ -approximation of its measure:*

$$\begin{aligned} \mu(A) &\leq \mu(E) + \epsilon, \\ A &= \bigcup_{j=1}^n R_j \supset E. \end{aligned}$$

*Proof.* From the definition of the Carathéodory outer measure, and the fact that it coincide with  $\pi$  on measure sets such as  $E$ , we have a countable cover  $R_1, R_2, \dots$  with:

$$\begin{aligned} \mu(\tilde{A}) &\leq \mu(E) + \frac{\epsilon}{2}, \\ \tilde{A} &= \bigcup_{j=1}^{\infty} R_j \supset E. \end{aligned}$$

Moreover, since  $\mu(E) < \infty$ , the sum can be truncated to provide a finite  $\epsilon$ -approximation. Finally, since  $\mathcal{A}$  is a semi-ring, we can rewrite the finite cover as a disjoint finite cover.  $\square$

**Lemma 2.** Let  $\pi_1, \pi_2$  be finite measures, and  $f$  a measurable function on the product  $\sigma$ -algebra  $\mathcal{F}_1 \otimes \mathcal{F}_2$ . Then for all  $\epsilon > 0$ , there is a measurable set  $B$  such that  $\pi_1 \otimes \pi_2(B) < \epsilon$ , and outside of which  $f$  is uniformly approximated by simple functions on rectangles:

$$\lim_{M \rightarrow \infty} \sup_{x \notin B} \left| f(x) - \sum_{m=1}^M c_m^M \mathbf{1}_{R_m^M}(x) \right| = 0,$$

for some  $R_m^M = F_m^M \times G_m^M$ ,  $F_m^M \in \mathcal{F}_1, G_m^M \in \mathcal{F}_2$ .

*Proof.* Assume  $f \geq 0$  (if not, apply this argument to the positive and negative parts of  $f$ ) then there exists simple functions  $f_M$  that converge almost everywhere to  $f$ :

$$\begin{aligned} \lim_{M \rightarrow \infty} f_M &= f \quad (\text{a.s.}) \\ f_M &= \sum_{m=1}^M c_m^M \mathbf{1}_{E_m^M}, \\ E_m^M &\in \mathcal{F}_1 \otimes \mathcal{F}_2 \end{aligned}$$

Next, we apply Lemma 1 to each  $E_m^M$ , with  $\mu = \pi_1 \otimes \pi_2$ . We set an exponentially decreasing tolerance  $\epsilon_m^M = \epsilon M^{-1} 2^{-M-1}$  so that:

$$\begin{aligned} \mu(A_m^M) &\leq \mu(E_m^M) + \epsilon M^{-1} 2^{-M-1}, \\ A_m^M &= \bigcup_{j=1}^{n_m^M} R_{m,j}^M \supset E_m^M. \end{aligned}$$

Note that outside of some bad set  $B_1$ , we now have pointwise convergence of simple functions on rectangles (since each  $A_m^M$  is a disjoint union of rectangles):

$$\begin{aligned} \lim_{M \rightarrow \infty} \sum_{m=1}^M c_m^M \mathbf{1}_{A_m^M} \Big|_{B_1^c} &= f \Big|_{B_1^c} \quad (\text{a.s.}) \\ B_1 &= \bigcup_{M=1}^{\infty} \bigcup_{m=1}^M (A_m^M \setminus E_m^M). \end{aligned} \tag{10}$$

Note that:

$$\begin{aligned} \pi_1 \otimes \pi_2(B_1) &\leq \sum_{M=1}^{\infty} \sum_{m=1}^M \epsilon M^{-1} 2^{-M-1} \\ &= \epsilon \sum_{M=1}^{\infty} 2^{-M-1} = \frac{\epsilon}{2}. \end{aligned}$$

Finally, pointwise convergence almost everywhere in Equation (10) implies by Egorov's theorem the existence of a set  $B_2$  with  $\pi_1 \otimes \pi_2(B_2) < \epsilon/2$  and such that convergence is uniform outside of  $B = B_1 \cup B_2$ .  $\square$

**Lemma 3.** *Suppose  $x < y + \beta_2$ . Then  $\mathbb{P}(|X - x| > \beta_1) < \alpha$  implies that  $\mathbb{P}(X > \beta_1 + \beta_2 + y) < \alpha$ .*

*Proof.* We prove that  $\mathbb{P}(X > \beta_1 + \beta_2 + y) < \mathbb{P}(|X - x| > \beta_1)$  via the contrapositive on the events:  $|X - x| \leq \beta_1 \implies X - x \leq \beta_1 \implies X \leq \beta_1 + \beta_2 + y$ .  $\square$

*Proof of Proposition 3.* Let us label the nodes of the tree using a *height function*  $h$  defined to be equal to zero at the leaves, and to  $h(t) = 1 + \max\{h(t_{t_1}), h(t_{t_2})\}$  for the internal nodes.

We proceed by induction on  $h = 0, 1, 2, \dots$ , showing that for all  $t$  such that  $h(t) \leq h$ , the normalized weighted particles  $(\mathbf{x}_{t,N}^i, \mathbf{W}_{t,N}^i)$  obtained from `dc_smc`( $t$ ) are consistent with respect to  $(\pi, \mathbf{C}_t)$ . The base case is trivially true. Suppose  $t$  is one of the subtrees such that  $h(t) = h$ . Note that its two children  $t_{t_1}$  and  $t_{t_2}$  are such that  $h(t_c) < h(t)$ , so the induction hypothesis implies these two children populations of weighted particles  $(\mathbf{x}_{t_1,N}^i, \mathbf{W}_{t_1,N}^i), (\mathbf{x}_{t_2,N}^i, \mathbf{W}_{t_2,N}^i)$  are consistent. We now show that we adapt Theorem 1 of DM08 to establish that the weighted particles  $(\mathbf{x}_{t,N}^i, \mathbf{W}_{t,N}^i)$  are consistent as well.

Note that for each simple  $f^M$  defined as in the proof of Lemma 2, we have:

$$\begin{aligned} & \sum_{i=1}^N \sum_{j=1}^N \mathbf{W}_{t_1,N}^i \mathbf{W}_{t_2,N}^j f^M(\mathbf{x}_{t_1,N}^i, \mathbf{x}_{t_2,N}^j) \\ &= \sum_{m=1}^M \left( \sum_{i=1}^N \mathbf{w}_{t_1,N}^i \mathbf{1}_{A_m^M}(\mathbf{x}_{t_1,N}^i) \right) \left( \sum_{j=1}^N \mathbf{w}_{t_2,N}^j \mathbf{1}_{B_m^M}(\mathbf{x}_{t_2,N}^j) \right) \\ &\xrightarrow{\mathbb{P}} \sum_{m=1}^M \left( \int \mathbf{1}_{A_m^M}(\mathbf{x}_{t_1}) \pi_{t_1}(d\mathbf{x}_{t_1}) \right) \left( \int \mathbf{1}_{B_m^M}(\mathbf{x}_{t_2}) \pi_{t_2}(d\mathbf{x}_{t_2}) \right) \\ &= \iint f^M(\mathbf{x}_{t_1}, \mathbf{x}_{t_2}) (\pi_{t_1} \otimes \pi_{t_2})(d\mathbf{x}_{t_1} \times d\mathbf{x}_{t_2}). \end{aligned} \quad (11)$$

Next, we show that this convergence in probability can be lifted from simple  $f^M$  to general bounded  $\mathcal{F}_{t_1} \otimes \mathcal{F}_{t_2}$ -measurable functions. To shorten the notation, let:

$$\begin{aligned} \mu_A(f) &= \pi_{t_1} \otimes \pi_{t_2}(\mathbf{1}_A f) \\ \mu_A^N(f) &= \sum_{i=1}^N \sum_{j=1}^N \mathbf{W}_{t_1,N}^i \mathbf{W}_{t_2,N}^j \mathbf{1}_A f(\mathbf{x}_{t_1,N}^i, \mathbf{x}_{t_2,N}^j), \end{aligned}$$

(and  $\mu(f), \mu^N(f)$  are defined similarly but without the indicator restriction).

Let  $\epsilon, \delta > 0$  be given. Using the result of Equation (11), first pick  $\underline{N} > 0$  such that for all  $N \geq \underline{N}$ ,  $\mathbb{P}(|\mu_{B^c}^N(f^M) - \mu_{B^c}(f^M)| > \epsilon) < \delta/2$ . Second, using Lemma 2 pick  $B \in \mathcal{F}_{t_1} \otimes \mathcal{F}_{t_2}$  and  $M > 0$  such that  $\sup_{\mathbf{x} \notin B} |f^M(\mathbf{x}) - f(\mathbf{x})| < \epsilon/C$  and  $\mu(B) < \epsilon/C$ . This implies that both  $|\mu_{B^c}(f^M) - \mu_{B^c}(f)|$  and  $|\mu_{B^c}^N(f^M) - \mu_{B^c}^N(f)|$  are bounded above by  $\epsilon$ . Third, using Lemma 1, pick a cover  $A$  of  $B$ , composed of a union of rectangles and such that  $\mu(A) < \mu(B) + \epsilon/C$ . Using Equation (11) again, pick  $\underline{N}' > 0$  such that for all  $N \geq \underline{N}'$ ,  $\mathbb{P}(|\mu^N(A) - \mu(A)| > \epsilon/C) < \delta/2$ . Applying Lemma 3 with  $X = \mu^N(A), \beta_1 = \beta_2 = \epsilon/C, x = \mu(A), \alpha = \delta/2$  and  $y = \mu(B)$ , we get  $\mathbb{P}(\mu^N(A) > 3\epsilon/C) < \delta/2$ .

From these choices, we obtain that for all  $N > \max\{\underline{N}, \underline{N}'\}$ :

$$\mathbb{P}(|\mu^N(f) - \mu(f)| > 4\epsilon) \leq \mathbb{P}(\mu_B^N(f) > 4\epsilon) + \mathbb{P}(D_1 + D_2 + D_3 + \mu_B(f) > 4\epsilon),$$

where:

$$\begin{aligned} D_1 &= |\mu_{B^c}^N(f) - \mu_{B^c}^N(f^M)| \\ D_2 &= |\mu_{B^c}^N(f^M) - \mu_{B^c}(f^M)| \\ D_3 &= |\mu_{B^c}(f^M) - \mu_{B^c}(f)|. \end{aligned}$$

Therefore:

$$\begin{aligned} \mathbb{P}(|\mu^N(f) - \mu(f)| > 4\epsilon) &\leq \mathbb{P}(\mu^N(B) > 4\epsilon/C) + \mathbb{P}(D_2 > \epsilon) \\ &\leq \mathbb{P}(\mu^N(A) > 3\epsilon/C) + \delta/2 \\ &\leq \delta. \end{aligned}$$

Next, we use the fact that resampling is performed at every iteration, Condition 4, and Theorem 3 from DM08, to view resampling as reducing the  $N^2$  particles into  $N$  unweighted particles. We plug in the following quantities in their notation:

$$\begin{aligned} M_N &= N^2 \\ \widetilde{M}_N &= N \\ \xi_{N,(i,j)} &= (\mathbf{x}_{t_1,N}^i, \mathbf{x}_{t_2,N}^j) \\ \omega_{N,(i,j)} &= \mathbf{W}_{t_1,N}^i \mathbf{W}_{t_2,N}^j. \end{aligned}$$

This yields that the  $N$  particles obtained from resampling  $N$  time from the particle approximation of  $\pi_{t_1} \times \pi_{t_2}$  creates a consistent approximation. Finally, Theorem 1 from DM08 closes the induction argument.  $\square$

## B D&C-SMC algorithm

In Algorithm 3 we provide pseudo-code for a more general D&C-SMC algorithm than what is given in Algorithm 2, specifically, incorporating mixture sampling (see Section 4.1) and tempering (see Section 4.2).

## C Supplement on the square-lattice MRF models

### C.1 Additional numerical results for the Ising model

In this section we provide some additional numerical results for the Ising model presented in Section 5.1 of the main text. First, in Figures 10–11 we repeat the results shown in Figure 6, but complemented with the estimates for D&C-SIR and D&C-SMC (mix).

Second, we have repeated the numerical evaluation described in Section 5.1 of the main text for different inverse temperatures of the Ising model:  $\beta = 0.40$  (90% of critical inverse temperature) and  $\beta = 0.48$  (110% of critical inverse temperature). The results are given in Figures 12–13 and Figures 14–15, respectively.



---

**Algorithm 3** `dc_smc(t)` – using mixture sampling and tempering
 

---

1. (a) For  $c \in \mathcal{C}(t)$ ,  $(\{\mathbf{x}_c^i, \mathbf{w}_c^i\}_{i=1}^N, \widehat{Z}_c^N) \leftarrow \text{dc\_smc}(c)$ .
- (b) For  $i = 1$  to  $N$ , draw  $(\check{\mathbf{x}}_{c_1}^i, \dots, \check{\mathbf{x}}_{c_C}^i)$  from

$$Q_t(d\mathbf{x}_{c_1}, \dots, d\mathbf{x}_{c_C}) = \sum_{i_1=1}^N \dots \sum_{i_C=1}^N \frac{v_t(i_1, \dots, i_C) \delta_{(\mathbf{x}_{c_1}^{i_1}, \dots, \mathbf{x}_{c_C}^{i_C})} (d\mathbf{x}_{c_1}, \dots, d\mathbf{x}_{c_C})}{\sum_{j_1=1}^N \dots \sum_{j_C=1}^N v_t(j_1, \dots, j_C)},$$

where

$$v_t(i_1, \dots, i_C) = \left( \prod_{c \in \mathcal{C}(t)} \mathbf{w}_c^{i_c} \right) \tilde{\pi}_t(\mathbf{x}_{c_1}^{i_1}, \dots, \mathbf{x}_{c_C}^{i_C}) / \prod_{c \in \mathcal{C}(t)} \pi_c(\mathbf{x}_c^{i_c}),$$

and where  $\tilde{\pi}_t$  is chosen by the user (e.g., according to (8)).

- (c) Compute

$$\widehat{Z}_t^N = \left( \prod_{c \in \mathcal{C}(t)} \widehat{Z}_c^N \left\{ \frac{1}{N} \sum_{i=1}^N \mathbf{w}_c^i \right\}^{-1} \right) \left\{ \frac{1}{N^C} \sum_{i_1=1}^N \dots \sum_{i_C=1}^N v_t(i_1, \dots, i_C) \right\}.$$

2. (a) For  $i = 1$  to  $N$ , if  $\tilde{\mathcal{X}}_t \neq \emptyset$ , simulate  $\tilde{\mathbf{x}}_t^i \sim q_t(\cdot | \check{\mathbf{x}}_{c_1}^i, \dots, \check{\mathbf{x}}_{c_C}^i)$  where  $(c_1, c_2, \dots, c_C) = \mathcal{C}(t)$ ; else  $\tilde{\mathbf{x}}_t^i \leftarrow \emptyset$ .
  - (b) For  $i = 1$  to  $N$ , set  $\mathbf{x}_{t,0}^i = (\check{\mathbf{x}}_{c_1}^i, \dots, \check{\mathbf{x}}_{c_C}^i, \tilde{\mathbf{x}}_t^i)$  and  $\mathbf{w}_{t,0}^i = 1$ .
  - (c) For SMC sampler iteration  $j = 1$  to  $n_t$ : (N.B.  $\gamma_{t,0} = \tilde{\pi}_t q_t$ .)
    - i. For  $i = 1$  to  $N$ , compute  $\mathbf{w}_{t,j}^i = \mathbf{w}_{t,j-1}^i \gamma_{t,j}(\mathbf{x}_{t,j-1}^i) / \gamma_{t,j-1}(\mathbf{x}_{t,j-1}^i)$ .
    - ii. Optionally, resample  $\{\mathbf{x}_{t,j-1}^i, \mathbf{w}_{t,j}^i\}_{i=1}^N$ :
      - Update  $\widehat{Z}_t^N \leftarrow \widehat{Z}_t^N \times \{\frac{1}{N} \sum_{i=1}^N \mathbf{w}_{t,j}^i\}$ .
      - Override the notation  $\{\mathbf{x}_{t,j-1}^i, \mathbf{w}_{t,j}^i\}_{i=1}^N$  to refer to the resampled particle system.
    - iii. For  $i = 1$  to  $N$ , draw  $\mathbf{x}_{t,j}^i \sim K_{t,j}(\mathbf{x}_{t,j-1}^i, \cdot)$  using a  $\pi_{t,j}$ -reversible Markov kernel  $K_{t,j}$ .
  - (d) For  $i = 1$  to  $N$ , set  $\mathbf{x}_t^i = \mathbf{x}_{t,n_t}^i$  and  $\mathbf{w}_t^i = \mathbf{w}_{t,n_t}^i$ .
3. Update  $\widehat{Z}_t^N \leftarrow \widehat{Z}_t^N \times \{\frac{1}{N} \sum_{i=1}^N \mathbf{w}_t^i\}$ .
  4. Return  $(\{\mathbf{x}_t^i, \mathbf{w}_t^i\}_{i=1}^N, \widehat{Z}_t^N)$ .
-

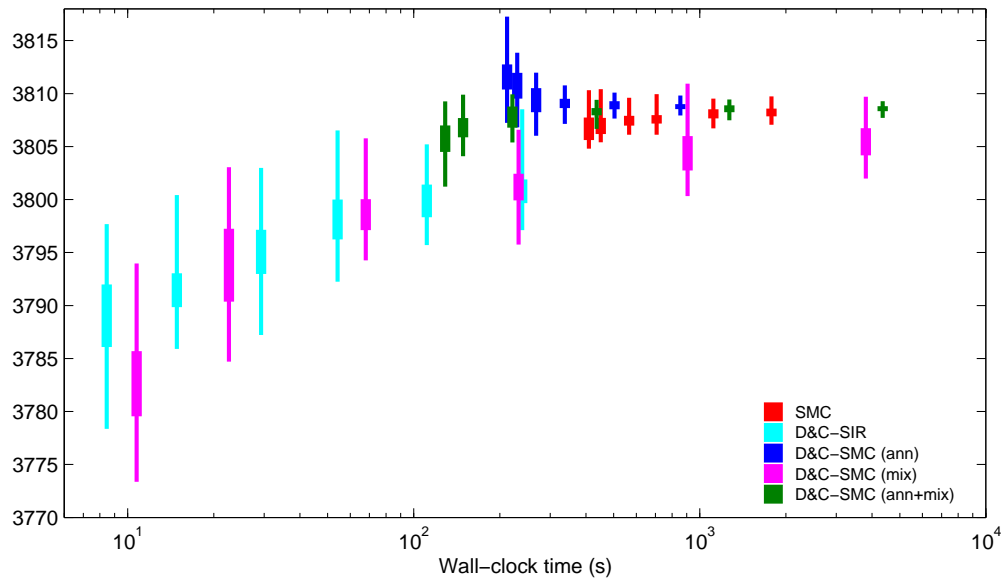


Figure 10: Box-plots (min, max, and inter-quartile) of estimates of  $\log Z$  for the Ising model with  $\beta = 0.44$  over 50 runs of each sampler (excluding single flip MH which does not readily provide an estimate of  $\log Z$ ). The boxes, as plotted from left to right, correspond to increasing number of particles  $N$ .

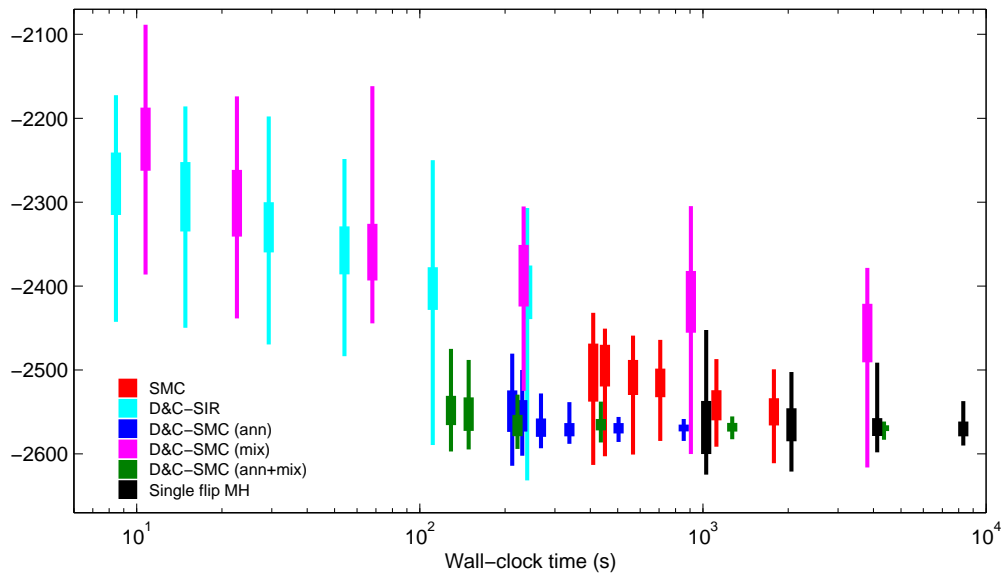


Figure 11: Box-plots (min, max, and inter-quartile) of estimates of  $\mathbb{E}[E(\mathbf{x})]$  for the Ising model with  $\beta = 0.44$  over 50 runs of each sampler. The boxes, as plotted from left to right, correspond to increasing number of particles  $N$  (or number of MCMC iterations for single flip MH).

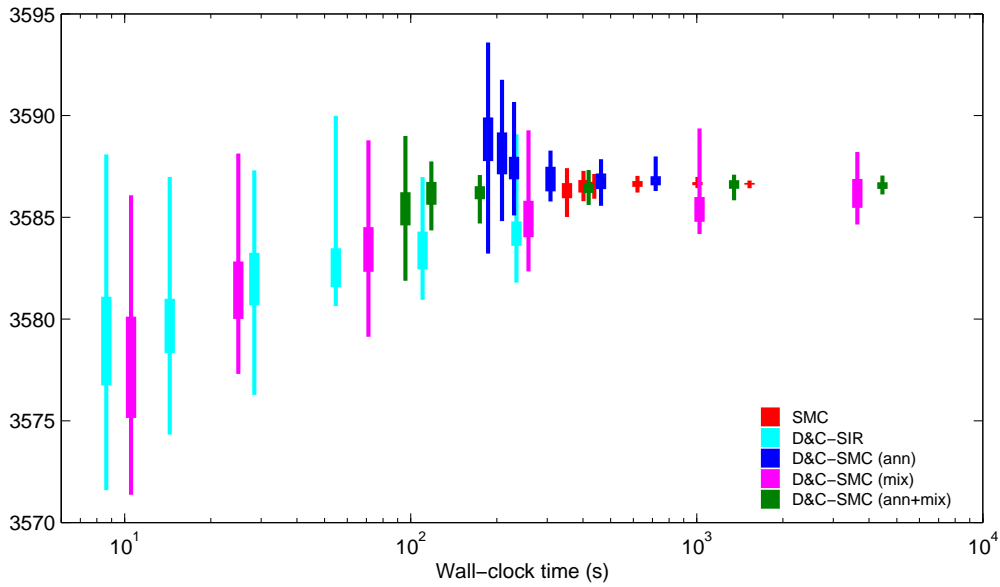


Figure 12: Box-plots (min, max, and inter-quartile) of estimates of  $\log Z$  for the Ising model with  $\beta = 0.40$  over 50 runs of each sampler (excluding single flip MH which does not readily provide an estimate of  $\log Z$ ). The boxes, as plotted from left to right, correspond to increasing number of particles  $N$ .

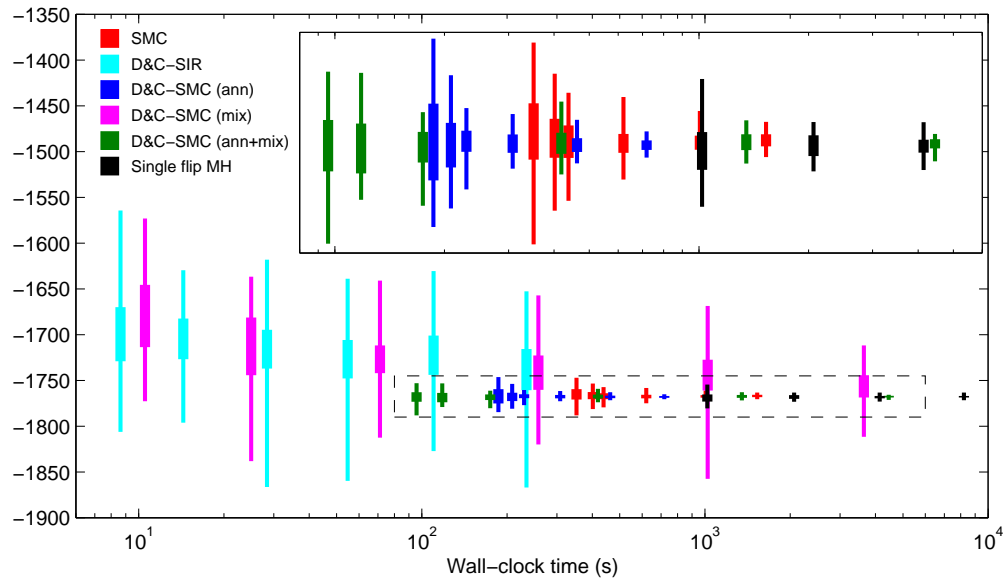


Figure 13: Box-plots (min, max, and inter-quartile) of estimates of  $\mathbb{E}[E(\mathbf{x})]$  for the Ising model with  $\beta = 0.40$  over 50 runs of each sampler. The boxes, as plotted from left to right, correspond to increasing number of particles  $N$  (or number of MCMC iterations for single flip MH). The overlaid axes is a zoom-in on the dashed region.

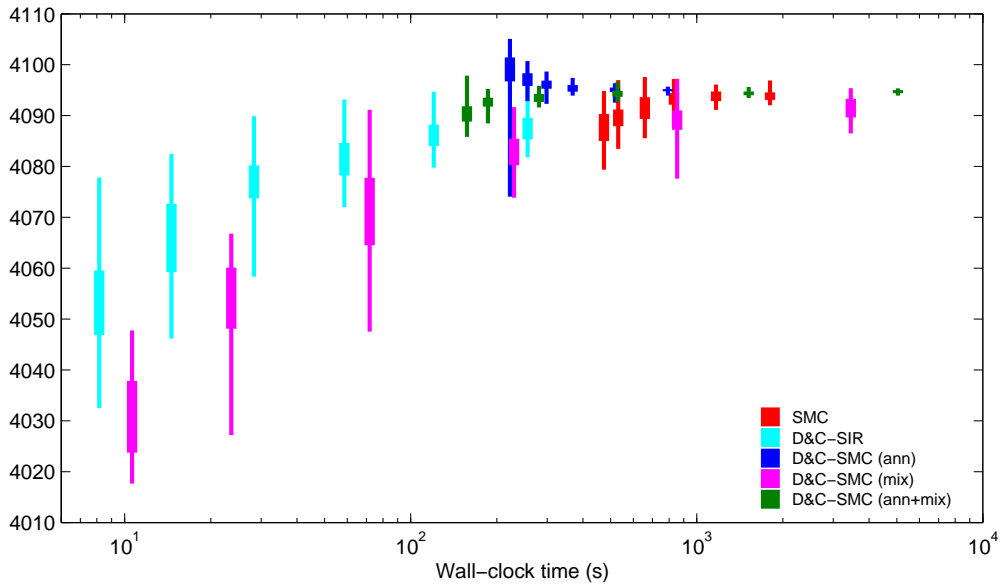


Figure 14: Box-plots (min, max, and inter-quartile) of estimates of  $\log Z$  for the Ising model with  $\beta = 0.48$  over 50 runs of each sampler (excluding single flip MH which does not readily provide an estimate of  $\log Z$ ). The boxes, as plotted from left to right, correspond to increasing number of particles  $N$ .

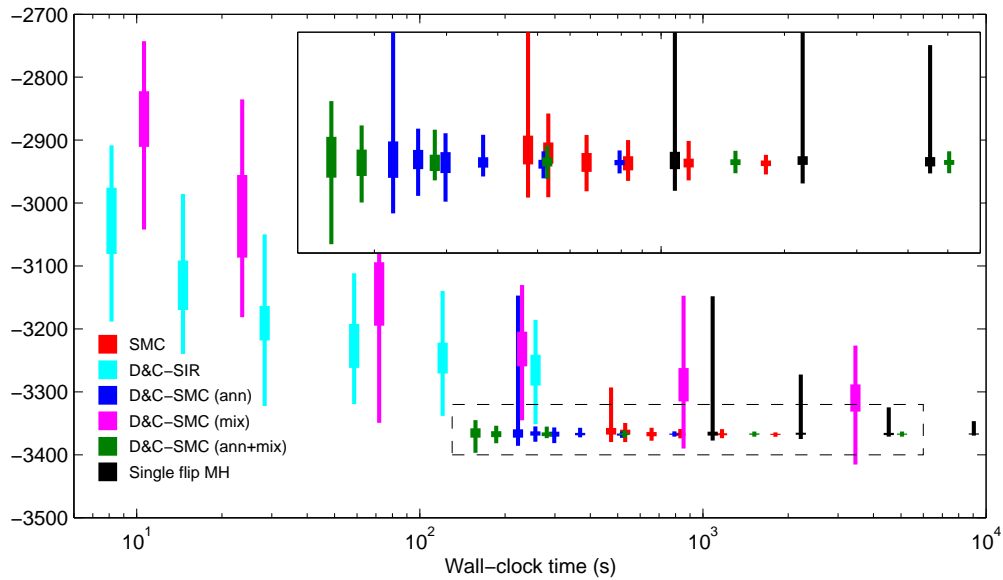


Figure 15: Box-plots (min, max, and inter-quartile) of estimates of  $\mathbb{E}[E(\mathbf{x})]$  for the Ising model with  $\beta = 0.48$  over 50 runs of each sampler. The boxes, as plotted from left to right, correspond to increasing number of particles  $N$  (or number of MCMC iterations for single flip MH). The overlaid axes is a zoom-in on the dashed region.

## C.2 Square-lattice MRF with continuous latent variables

In this section we evaluate the proposed D&C-SMC method on a second square-lattice MRF example. We consider a toy-model consisting of a latent Gaussian field  $\mathbf{x} \in \mathbb{R}^{M \times M}$  ( $M = 32$ ), with nearest-neighbour interactions and periodic boundary conditions:

$$p(\mathbf{x}) \propto \exp \left( -\frac{1}{2} \left\{ \sum_{(k,\ell) \in \mathcal{E}} \lambda_1 (x_k - x_\ell)^2 + \lambda_2 \sum_{k \in \mathcal{V}} x_k^2 \right\} \right), \quad (12)$$

with  $\mathcal{E}$  and  $\mathcal{V}$  being the edge set and vertex set of the MRF, respectively. We set  $\lambda_1 = 10$  and  $\lambda_2 = 0.01$  for the interaction strength and node potential, respectively. To each node of the MRF we also attach an observed variable  $y_k$ , conditionally distributed according to  $p(y_k | x_k) = \mathcal{N}(y_k | x_k^2, 0.05^2)$ ,  $k \in \mathcal{V}$ . The target distribution for the samplers is then given by the Bayesian posterior distribution  $p(\mathbf{x} | \mathbf{y})$ , where  $\mathbf{y} = \{y_k\}_{k \in \mathcal{V}}$ .

We simulate a batch of data from the model and apply the same inference methods as used in Section 5.1 to sample from the posterior distribution. We initialise all methods by sampling independently for each  $k \in \mathcal{V}$  from a distribution given by,

$$\mu_k(x_k) \propto N(y_k | x_k^2, 0.05^2) \exp \left( -\frac{\lambda_2}{2} x_k^2 \right), \quad (13)$$

which we compute to high precision by (one-dimensional) adaptive quadrature. This allows us to focus the evaluation on the difficulties arising from the interactions between neighbouring sites, since (13) is exactly the posterior distribution of  $x_k$  if we neglect all interactions. Note that we observe the square of the latent variables  $x_k$  (plus noise). Consequently, the distributions (13), as well as the marginal posteriors  $p(x_k | \mathbf{y})$ , tend to be bimodal whenever  $|x_k|$  is large (relative to the observation variance). This poses significant difficulties for the single site MH sampler and the standard SMC sampler, as we shall see below.

All algorithmic settings are the same as in Section 5.1, with the exception that the MCMC kernel used for the annealed methods (and for the single site MH sampler) uses a Gaussian random walk proposal with standard deviation 0.132 (chosen by manual tuning; we obtained an average acceptance rate of 0.6–0.7 for all methods). It is interesting to note that we only needed to make small modification to the code used for the Ising model, changing only the initialisation procedure, the energy function, and the MCMC kernel.

Figures 16 and 17 show results on the estimates of the log-normalising-constant and the expected energy for the posterior distribution, obtained from 50 runs of each algorithm on a single data set. The results for the single site random-walk MH sampler are not shown since the method fails completely to converge to samples from the correct posterior distribution (inter-quartile range in the estimates of the expected energy over the 50 independent runs of the MCMC sampler is more than 7000; cf., Figure 17).

We also note a superior performance of all D&C-SMC samplers compared to SMC, which is attributed to the fact that the D&C-SMC samplers are better able to handle the multimodality of the initial distributions than the “standard” SMC approach considered: in standard SMC we initialise a single particle population by simulating  $N$  times from the product measure  $\otimes_{k \in \mathcal{V}} \mu_k(dx_k)$ , where  $\mu_k$  is given by (13). Since many of the  $\mu_k$ ’s are expected to be multimodal, this will likely result in particles that have very low posterior probability under

the “correct model” (i.e., with the interactions taken into account). Indeed, any neighbouring pair  $(x_k, x_\ell)$  where  $x_k$  is drawn from the “positive mode” and  $x_\ell$  is drawn from the “negative mode” will have low probability under the prior (12). Furthermore, since we use local MCMC moves to update the particle positions, the method is not able to correct for this in a sufficiently efficient manner during the annealing process. The D&C-SMC samplers are much better suited to handling this difficulty, since they make use of *multiple* particle populations at initialisation, one for each site. The interactions are thereafter gradually taken into account in the merge steps of the algorithm. This improvement comes without any application-specific implementation effort.

To further illustrate the ability of D&C-SMC to capture the multimodality of the marginal posteriors, we show in Figure 18 the empirical cumulative distribution functions for the samplers for four sites with increasing  $|x_k|$ . The results are for  $N = 2048$  ( $N = 32768$  for D&C-SIR) and each line correspond to one of the 50 independent runs. It is clear that the D&C-SMC samplers maintains the multimodality of the posterior much better than standard SMC.

## D Supplement on the hierarchical Bayesian model data analysis

### D.1 Data pre-processing

The data was downloaded from <https://data.cityofnewyork.us/Education/NYS-Math-Test-Results-By-Grade-2006-2011-School-Le/jufi-gzgp> on May 26, 2014. It contains New York City Results on the *New York State Mathematics Tests*, Grades 3-8. We used data from grade 3 only.

Data is available for the years 2006–2011. We removed years 2010 and 2011, since the documentation attached to the above URL indicates that: “Starting in 2010, NYSED changed the scale score required to meet each of the proficiency levels, increasing the number of questions students needed to answer correctly to meet proficiency.”

Each row in the dataset contains a school code, a year, a grade, the number of students tested, and summary statistics on their grades. We use the last column of these summary statistics, which corresponds to the number of students that obtained a score higher than a fixed threshold.

Moreover, for each school code, we were able to extract its school district. We removed the data from the schools in School District 75. This is motivated by the specialized character of School District 75: “District 75 provides citywide educational, vocational, and behavior support programs for students who are on the autism spectrum, have significant cognitive delays, are severely emotionally challenged, sensory impaired and/or multiply disabled.” (<http://schools.nyc.gov/Academics/SpecialEducation/D75/AboutD75/default.htm>)

For each school district we can also extract its county, one of Manhattan, Bronx, Kings, Queens, Richmond (note that some of these correspond to NYC boroughs with the same name, while Kings corresponds to Brooklyn; Richmond, to Staten Island; and Bronx, to The Bronx). The pre-processing steps can be reproduced using the script `scripts/prepare-data.sh` in the repository.

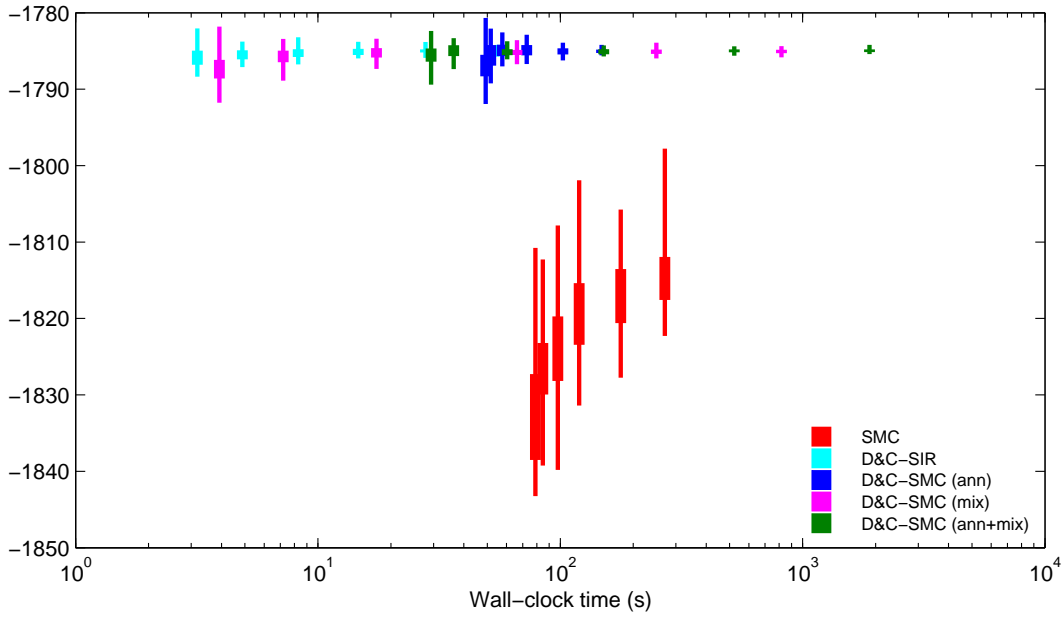


Figure 16: Box-plots of estimates of  $\log Z$  over 50 runs of each sampler. The boxes, as plotted from left to right, correspond to increasing number of particles  $N = 2^6$  to  $2^{11}$  ( $N = 2^{10}$  to  $2^{15}$  for D&C-SIR). The overlaid axes is a zoom-in on the dashed region.

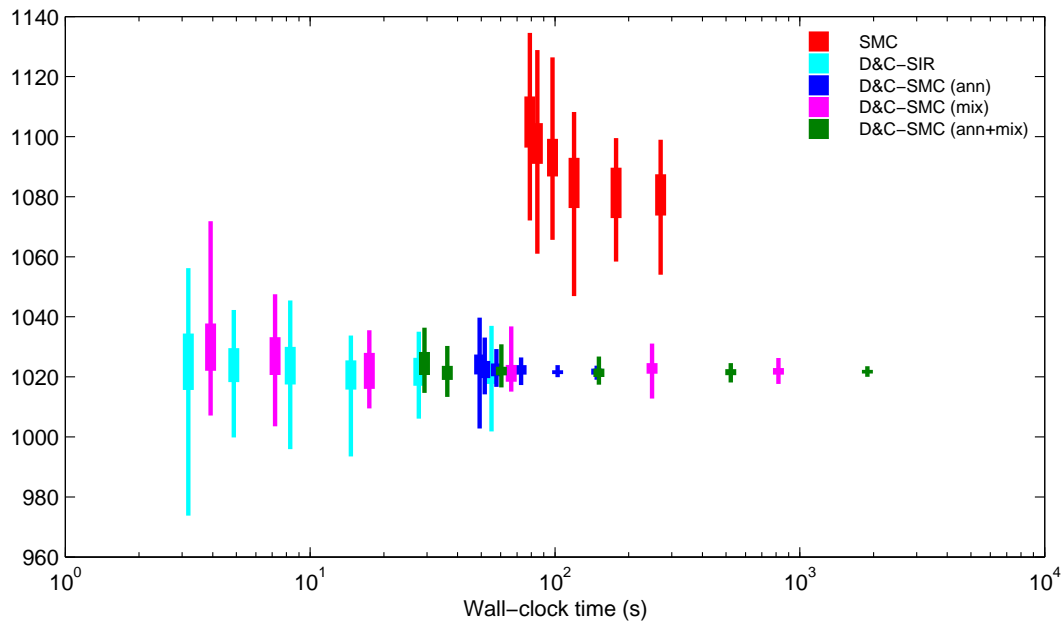


Figure 17: Box-plots of estimates of  $\mathbb{E}[E(\mathbf{x})]$  over 50 runs of each sampler. The boxes, as plotted from left to right, correspond to increasing number of particles  $N = 2^6$  to  $2^{11}$  ( $N = 2^{10}$  to  $2^{15}$  for D&C-SIR). The overlaid axes is a zoom-in on the dashed region.

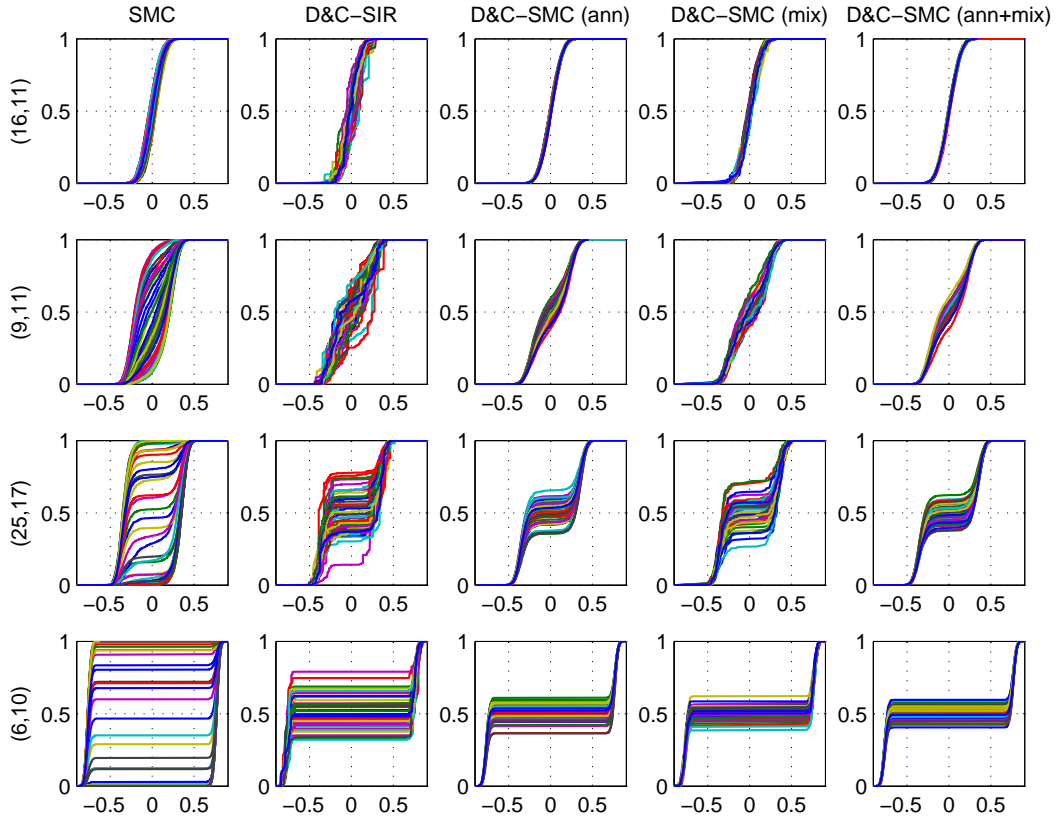


Figure 18: Empirical cumulative distribution functions for the marginal posteriors  $p(x_k | \mathbf{y})$  for four sites with increasing  $|x_k|$  (from top to bottom). Each line correspond to one of the 50 independent runs of each algorithm.



## D.2 Additional information on the experimental setup

We checked correctness of the implementations by verifying on small examples that the posterior distributions obtained from all four methods (the three baselines and ours) become arbitrarily close when increasing the number of particles or MCMC iterations. We also subjected our Gibbs implementation to the Prior/Prior-Posterior correctness test of Geweke (2004).

The precise command line arguments used in the experiments as well as the scripts used for creating the plots can be found at <https://github.com/alexandrebourchard/multilevelSMC-experiments>. To describe in more detail the methods we compared to, we introduce the following notation: given a permutation  $t_1, t_2, \dots$  of the index set  $T$ , we set  $\Xi_j$  to  $\theta_{t_j}$  if  $t_j$  is a leaf, or to  $\sigma_{t_j}^2$  otherwise. The three baseline methods are:

**Gibbs:** A Metropolis-within-Gibbs algorithm, proposing a change on a single variable, using a normal proposal of unit variance. As with D&C-SIR, we marginalize the internal  $\theta_t$  parameters. More precisely, we first sample a permutation  $t_1, t_2, \dots$  uniformly at random, then using the Metropolis-within-Gibbs kernel, we sample  $\Xi_1$ , followed by  $\Xi_2$ , and so, until we sample  $\Xi_{|T|}$ , at which point we sample an independent permutation uniformly at random and restart the process. The Java implementation is available at <https://github.com/alexandrebourchard/multilevelSMC>, in the package “multilevel.mcmc”. We use a burn-in of 10% and collect sample each time we resample a permutation of the nodes.

**Stan:** An open-source implementation of the Hamiltonian Monte Carlo algorithm (Neal, 2011), more precisely of the No U-Turn Sampler (Hoffman and Gelman, 2012), which adaptively selects the number of “leap frog” steps. Stan generates efficient C++ code. In contrast to the other methods, we did not implement marginalization of the internal  $\theta_t$  parameters. Stan includes a Kalman inference engine, however it is limited to chain-shaped graphical models as of version 2.6.0. We use the default setting for the burn-in and adaptation period (50%) and a thinning of 10.<sup>6</sup>

**STD:** A standard (single population) bootstrap filter with the intermediate distributions being sub-forests incrementally built in post-order. More precisely, let  $t_1, t_2, \dots$  denote a fixed post-order traversal of the nodes in the set  $T$ . Note that a prefix of this traversal,  $t_1, t_2, \dots, t_k$ , corresponds to a forest, with a corresponding parameter vector  $\Xi_{1:k} = (\Xi_1, \Xi_2, \dots, \Xi_k)$ . We use a standard SIR algorithm to sample  $\Xi_{1:1}, \Xi_{1:2}, \Xi_{1:3}, \dots$ , using the canonical sequence of intermediate distributions. Again, as with D&C-SIR, we marginalize the internal  $\theta_t$  parameters. To propose an additional parameter  $\Xi_i$  given its children, we use the same proposal distributions as those we used for D&C-SIR (described in Section 5.2 of the main text). The Java implementation is available at <https://github.com/alexandrebourchard/multilevelSMC>, in the package “multilevel.smc”.

---

<sup>6</sup>In other words, we store one sample every 10 accept-reject rounds. Since a large number of Hamilton Monte Carlo iterations was needed, this was useful to decrease storage. We verified using an ACF plot that this did not significantly penalize this method.

### D.3 Additional results (serial)

We show in Figure 19 the posterior densities of the parameters  $\sigma_t^2$ , for  $t$  ranging in the nodes in the two top levels of the tree, and for the four methods with different numbers of particles or MCMC iterations. The plots support that 1 000 particles are sufficient for D&C-SMC to output a reasonable approximation (see rows DC- $N$ ), while a larger number of MCMC iterations seem required for Gibbs (GIBBS- $N$ ) or Stan (STAN- $N$ ). Note however that DC- $N$  and STD- $N$  performed similarly in this first set of results.

Next, we show in Figure 20 a comparison of the wall clock times for the different algorithm configurations. These experiments were performed on Intel Xeon E5430 quad-core processors, running at 2.66 GHz. While the detailed rankings of the methods are implementation and architecture dependent, the results show that the DC-1 000 was computed in approximately one minute, while all the reasonably mixed MCMC methods required at least one order of magnitude more time. For example, running 2 000 Stan iterations (1 000 burn-in + 1 000 samples) took around 6 hours. All Stan running times exclude the one-time model compilation.

The results for both SMC and MCMC are all performed on a single thread. We attribute the high computational efficiency of the SMC methods to the favorable memory locality of the particle arrays. This is supported by the non-linearity of the running time going from 1000 to 10 000 particles (the theoretical running time is linear in the number of particles).

Note that for any given particle budget, our implementation of D&C-SMC was slightly faster than STD. This could be caused by implementation details related to the fact that the particle datastructure for D&C-SMC are simpler than those required by STD (the particles being forests in STD, instead of trees for D&C-SMC).

These results further demonstrate that the model and data used in this section yield a challenging posterior inference problem.

### D.4 Additional results (distributed)

In this section, we provide a proof-of-concept demonstrating the suitability of D&C-SMC to distributed computing environments (supplementing the discussion in Section 5.3 of the main text).

In this discussion, it is useful to emphasize the usual distinction between *parallel* architectures, where a single computer is composed of several cores sharing fast access to memory, and *distributed* architectures, where several computers (nodes) are connected by a relatively slower network.

Parallelizing SMC is typically done in the proposal step, at the granularity of particles: when sampling from  $q$  or reweighting is expensive, or both, it becomes advantageous to parallelize these operations. However, the resampling step requires frequent communication, making this strategy less attractive in a distributed setting (but see for example Bolic et al. (2005); Jun et al. (2012); Vergé et al. (2014); Lee and Whiteley (2014); Whiteley et al. (2015) for alternatives).

In contrast, distributed computation in D&C-SMC can be scheduled to incur low communication costs. The main idea is to split the work at the granularity of populations, instead of the more standard particle granularity. In the following, we describe a simple strategy

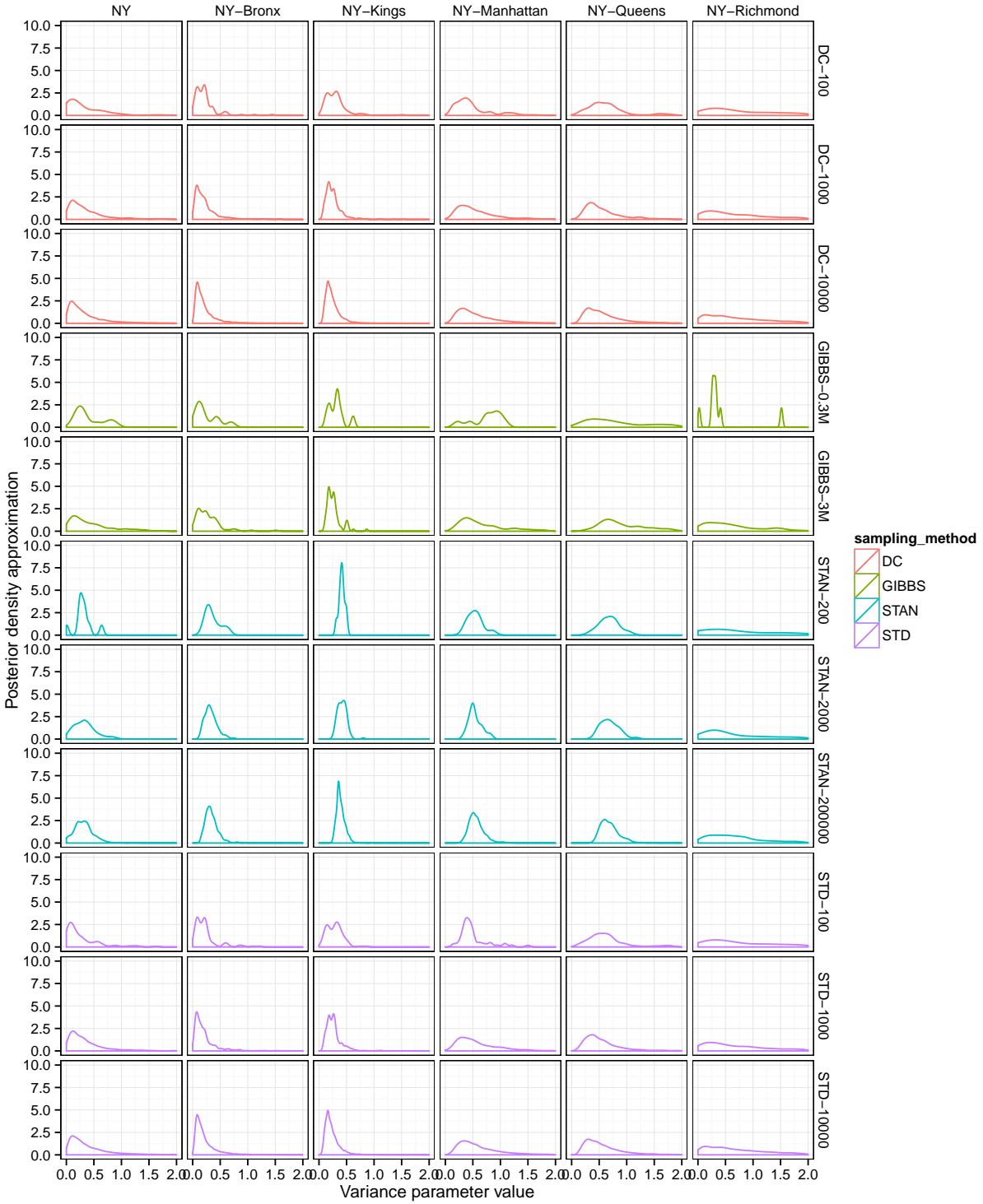


Figure 19: Posterior densities for the parameters  $\sigma_t^2$ . The rows index different methods and numbers of particles/iterations. The columns index different parameters  $t$  (only the first two levels shown).

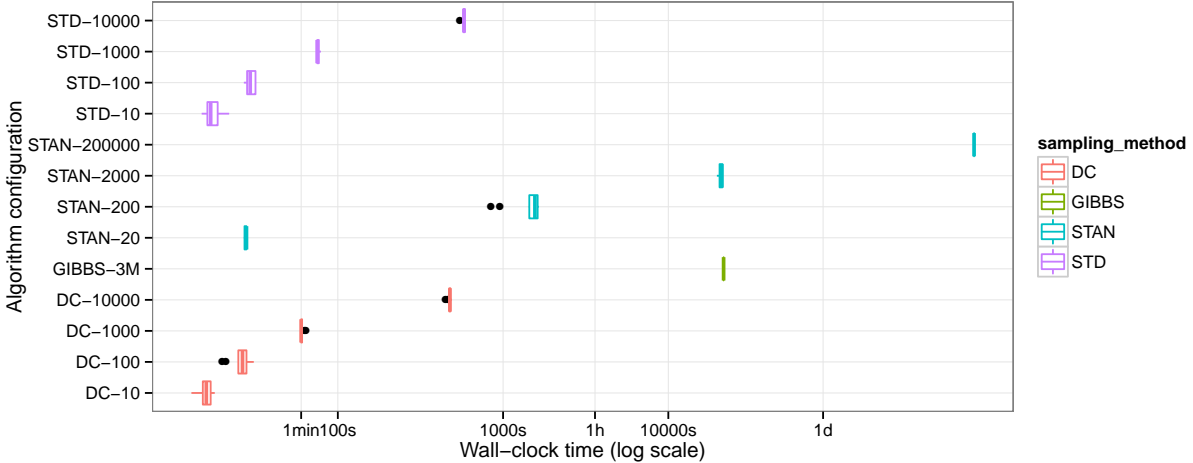


Figure 20: Comparison of the wall clock times for the different algorithm configurations. Note that the time axis is in log scale, and that iterations/particles were incremented exponentially. All experiments were replicated 10 times (varying only the Monte Carlo random seed), with the exception of the largest experiments taking more than 6 hours, which we ran only once (GIBBS-3M and STAN-200000).

to decrease communication costs when the D&C-SMC recursion is computed in parallel at several locations of the tree  $t \in T$ . To simplify the exposition, we assume that the tree is binary.

To describe our distribution strategy, we introduce the notion of the *depth* of a vertex in the tree  $t \in T$ . We set the depth to be zero at the root  $r$ ,  $\text{depth}(r) = 0$ , and recursively, for each vertex  $v$  with parent  $v'$ ,  $\text{depth}(v) = \text{depth}(v') + 1$ . We consider the largest depth  $d$  such that the number of vertices at that depth is greater or equal to the number  $c$  of compute nodes available. For each vertex  $v$  such that  $\text{depth}(v) = d$ , we assign the computation of all the D&C-SMC recursions for the vertices under  $v$  to the same computer.

With this architecture, communication is only required at edges of the tree  $T$  connecting nodes above depth  $d$ . This implies that the number of particles transmitted over the network will be  $O(cN)$ . In contrast, naively distributing using a particle granularity would require  $O(c|T|N)$  particle transmissions. Moreover, the population granularity strategy can be done in a completely decentralized fashion.

Based on this method, we have implemented an open source library for performing distributed, decentralized D&C-SMC computation. Thanks to its decentralized nature, the package is simple to use: nodes discover each other automatically and only require a rough estimate on the number of nodes available, to specify the value  $d$  discussed above. However, the algorithm is fault tolerant, in the sense that if some of the compute nodes fail, the computation will still be completed.

We applied this algorithm to the New York Mathematics Test dataset. We varied the number of active nodes in the cluster in  $\{1, 2, 4, 8, 16, 32\}$ , using 100 000 particles in all cases. The output of the distributed algorithm is identical in all cases, so it suffices to compare wall-clock times. The compute nodes consist in Xeon X5650 2.66GHz processors connected by a non-blocking Infiniband 4X QDR network. We show the results in Figure 21.

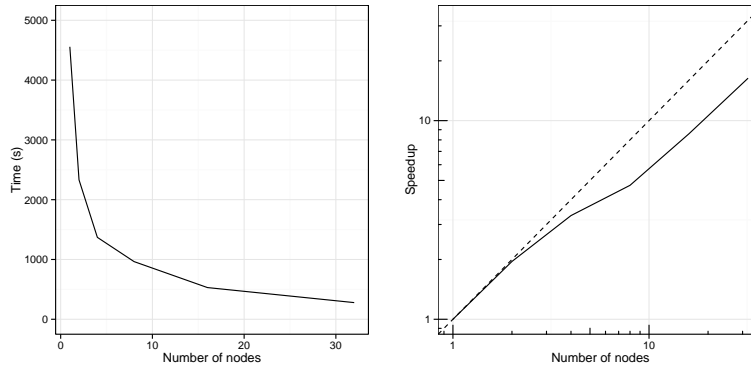


Figure 21: (a) Wall-clock times for the distributed D&C-SMC algorithm. (b) Speedup for the distributed D&C-SMC algorithm (log scale).

Each node used a single thread for simplicity, but note that combining parallelism and distribution can be done by parallelizing either at the level of particles, or populations with depths greater than  $d$ .